A strategic approach of enzyme engineering by attribute ranking and enzyme immobilization on zinc oxide nanoparticles to attain thermostability in mesophilic Bacillus subtilis lipase for detergent formulation

Mohd Faheem Khan, Debasree Kundu, Chinmay Hazra, Sanjukta Patra

PII: S0141-8130(19)31788-X
DOI: https://doi.org/10.1016/j.ijbiomac.2019.06.042
Reference: BIOMAC 12548

To appear in: *International Journal of Biological Macromolecules*

Received date: 9 March 2019
Revised date: 6 June 2019
Accepted date: 7 June 2019

Please cite this article as: M.F. Khan, D. Kundu, C. Hazra, et al., A strategic approach of enzyme engineering by attribute ranking and enzyme immobilization on zinc oxide nanoparticles to attain thermostability in mesophilic Bacillus subtilis lipase for detergent formulation, International Journal of Biological Macromolecules, https://doi.org/10.1016/j.ijbiomac.2019.06.042

A strategic approach of enzyme engineering by attribute ranking and enzyme immobilization on zinc oxide nanoparticles to attain thermostability in mesophilic *Bacillus subtilis* lipase for detergent formulation

Mohd Faheem Khan[1], Debasree Kundu[1], Chinmay Hazra[2] and Sanjukta Patra[1*]

[1]Department of Biosciences and Bioengineering, Indian Institute of Technology Guwahati, Guwahati-781039, Assam, India

[2]Department of Biotechnology, Indian Institute of Technology Kharagpur, Kharagpur-721302, West Bengal, India

[*]Corresponding author

Phone: [+91-361-258-2213]

Fax: [+91-361-258-2249]

E-mail: sanjukta@iitg.ac.in

Abstract

The present study envisaged rationalized protein engineering approach to attain thermostability in a mesophilic *Bacillus subtilis* lipase. Contributing amino acids for thermostability were analyzed from homologous thermophilic-mesophilic protein dataset through relative abundance and generated ranking model. Analyses divulged priority of charged amino acids for thermostability. Ranking model was used to predict thermostabilizing mutations. Three lipase mutants, bsl_the1 (V149K, Q150E), bsl_the2 (F41K, W42E, V149K, Q150E) and bsl_the3 (F41K, W42E, P119E, Q121K, V149K, Q150E) were generated and validated through *in silico* and *in vitro* approaches for improved activity and thermostability. ZnO nanoparticles were synthesized by precipitation method and functionalized using polyethylenimine, APTES and glutaraldehyde for lipase immobilization. The immobilization was confirmed through various analytical techniques. Analysis revealed bsl_wt showed optimum activity at 35 °C and pH 8 which was increased to 60 °C and pH 10 in case of ZnO-bsl_the3. The ZnO-bsl_the3 showed 80 % of their initial activity after 60 days of storage stability and retained 78 % of activity after 20 cycles of reuse. Lipases were applied for oil and grease stain removal from fabric. ZnO-bsl_the3 removed 90 % and 82 % of oil and grease stains, respectively. Conclusively, it revealed a promising perspective of low-cost nanobiocatalysts in detergent formulation.

Keywords

Protein engineering; Thermostability; Immobilization

1. Introduction

Enzymes are catalytic proteins having absolute selectivity, specificity and can act as green alternative replacing conventional chemical catalysts [1]. Since last two decades, enzymes have found increased application in various industrial sectors [2]. Amongst different industries, enzymes provide remarkable benefits in detergent formulations by reducing energy consumption through shorter washing times, less water consumption, and reduced chemical load. To enhance the cleaning ability of detergents, enzymes such as proteases, lipases, amylases, etc. are excessively used in detergent formulations to remove tough stains and make them environment friendly. Lipases are one such hallmark enzymes that can easily remove greasy and oily stains from the fabrics and act as a potential additive that exhibits better stability towards commercial detergents [3]. However, thermostability and alkaline tolerance of lipases is the major concern for their commercialization as detergent additive [4]. This necessitates the development of thermo-alkaline tolerant lipase to sustain activity even at harsh detergent conditions. Till date, various techniques are employed to attain thermostability of enzymes such as protein engineering, enzyme immobilization, etc. [5]. Protein engineering is the most promising aspect and provides improved properties to the proteins. Majorly, it is classified into two categories; random mutagenesis/directed evolution and rational protein design/computer-aided protein engineering [6]. Directed evolution provides genetic diversification, library screening and selection. The major drawback of this method is that it requires robust screening and selection of the mutants for desired characteristics making it time consuming and cost-intensive. However, the present rationalized protein engineering approach integrates computer-aided, rapid and potential method for predicting stability of the designed mutations [7]. Therefore, the novelty of

the present research lies in moving from random mutagenesis to a pre-predicted rationalized protein engineering platform by ranking the contributing protein attributes of thermostability.

To increase the thermostability of proteins through rationalized approach, the flexible sites need to be predicted and rigidified. The flexible sites have less number of interactions with local amino acids which triggers unfolding of proteins due to thermal fluctuations [5,8]. Thermostability thus, can be enhanced by substituting these amino acids with those that increases non-covalent interactions (hydrogen bonds, ionic interactions, salt-bridges, hydrophobic interactions) between contact residues. This necessitates the search for mutable hotspots in the flexible region using *in silico* prediction to compute the effects of mutations in such regions on stability changes in proteins [8,9]. In the process, the chosen mutable residues should not belong to any stabilizing centre(s) and active site pocket(s). Thus, mutations should be done on the loop regions and surface exposed regions for improving thermostability [10,11]. The mutable hotspots identified are designed for *in silico* mutagenesis followed by experimental validation through site-specific mutagenesis. However, these mutable residues play crucial role in attaining thermostability, so it is imperative to identify the specific amino acids and their preference for protein thermostability. The present approach is an attempt that involves amino acids prioritization to select the favored mutations for thermostability.

Another additional stabilization approach that can function in combination to protein engineering is enzyme immobilization. Enzymes are capable of working at room temperature. However, immobilized enzymes have the advantages of exhibiting better activity, specificity, thermostability, storage stability and reusability as compared to free enzymes [12]. The improved performance of immobilized enzymes are dependent upon multipoint attachment with support, structure of the support, properties of the spacer, microenvironment of the immobilization carrier

and immobilization conditions [12,13]. Amongst various methods and carriers for immobilization, nanoscale carriers offer a versatile technology that provides large surface areas to load more enzyme and reduces mass transfer resistance for substrates. However, when immobilized in non-porous nanomaterials, enzyme molecules are located in the external surface of the support which poses problems such as exposure of the enzyme to hydrophobic interfaces and interaction of enzyme molecules in one nanoparticle with the enzyme molecules in other nanoparticle. To prevent such difficulties, the immobilized support is often coated with a polymer [14]. Thus, it is essential to carefully design the optimal enzyme immobilization strategy for various industrial processes. Use of glutaraldehyde as the crosslinker has the broadest applicability as a versatile tool in enzyme immobilization [15–17]. Moreover, for lipases, immobilization through glutaraldehyde cross-linking on NH_2-active supports in presence of detergents can improve enzyme performance as well as increase their activity. This is because detergents shift lipase conformation towards the open form in the aqueous media permitting hydrophobic active site accessible to the hydrophobic substrate through interfacial activation of the enzyme [18,19].

In an attempt to attain thermostability in a mesophilic enzyme through a strategic approach, the amino acids rendering thermostability were ranked and knowledge-based site-specific mutations were predicted. Thus, this study makes an effort to (a) identify the contributing amino acid attributes, (b) rank them for their preferences to attain enzyme thermostability employing *in silico* designing approaches followed by validation through *in vitro* mutagenesis, and (c) immobilization of the improved engineered biocatalyst onto zinc oxide (ZnO) nanoparticles for enzymatic detergent formulation. In a nutshell, the present study aims at converging rationalized protein engineering and enzyme immobilization approaches to put forth an integrated nano-

immobilized enzyme engineering system for enhancing thermostability thereby, increasing its applicability in detergent industry.

2. Materials and Methods

2.1 Bacterial strains and chemicals

Escherichia coli DH5α and BL21(DE3) (Invitrogen, USA) were used for cloning and protein overexpression, respectively and cultured in Luria-Bertani (LB) medium (Merck, USA). The plasmid pET-28a(+) from Addgene (USA) was used for recombinant enzyme production. Quick Ligation^{TM} kit, BamHI, NdeI, DNA and protein markers were purchased from New England Biolabs (UK). StrataPrep Plasmid Miniprep Kit, StrataPrep DNA Gel Extraction Kit, QuikChange Site-Directed Mutagenesis Kit and SYPRO orange dye were purchased from Agilent Technologies (USA). Ni-NTA resin and polypropylene columns were obtained from Qiagen (USA) for His-tagged enzyme purification. Reagents such as kanamycin sulphate, *p*-nitrophenyl octanoate (*p*-NPO), polyethyleneimine (PEI), (3-aminopropyl) triethoxysilane (APTES) and glutaraldehyde (25%, aqueous solution) were purchased from Sigma-Aldrich (Germany). Zinc sulphate ($ZnSO_4$), sodium hydroxide (NaOH), surfactants (Tween 20; Tween 80; Triton X-100; NP-40 and sodium dodecyl sulfate, SDS), oxidizing agents (hydrogen peroxide, H_2O_2; sodium perborate, $NaBO_3$ and sodium hypochlorite, NaOCl) were procured from Hi-Media (India). Commercial detergents like Ariel, Surf Excel, Henko, Tide and Vanish were used for fabric destaining. All other reagents, solvents used were of molecular biology/analytical grade and obtained from Merck (USA) and Himedia (India).

2.2 Data collection and generation of contributing amino acids for thermostability

Thermophilic protein sequences were collected from UniProtKB and filtered for non-redundancy with the removal of partial and putative proteins. Homologous mesophilic proteins were

searched for each thermophilic proteins using BLASTp program (Table S1). Amino acid compositions were determined from collected thermophilic and mesophilic proteins using PEPSTATS. Data pertaining to amino acid compositions were subjected to non-parametric two-sample Kolmogorov-Smirnov (KS) test using MATLAB. It filtered statistically significant amino acids by p-value ≤ 0.05. The final datasets consisted of only statistically significant amino acids. It was used for computing relative abundance and generating ranking model for amino acids contributing to protein thermostability.

2.3 Computing relative abundance of amino acids in thermophiles and mesophiles

Relative abundance of significant amino acids were computed for understanding their preference either to thermophilic proteins or to mesophilic proteins. The weighted average of significant amino acids for each protein were calculated followed by calculating the difference in the weighted averages of those amino acids from thermophilic proteins *w.r.t.* mesophilic proteins. Each weighted average difference for a significant amino acid was normalized with the highest valued weighted average difference that resulted into enumeration of relative abundances of statistically significant amino acids. Mathematically, relative abundance was calculated using derived equation described earlier [20].

2.4 Ranking of amino acids for thermostability

Analytic hierarchical process (AHP) is a multi-criteria decision-making (MCDM) method that was applied as a prediction method to rank the amino acids contributing to protein thermostability. The method comprised of three hierarchies namely, goal, criteria and alternative. Here, the goal was to predict thermostabilizing mutations based on ranking of significant amino acids as criteria and to validate the generated model through thermophilic and mesophilic proteins as alternatives. Fig. S1 of the Supplementary Information details out the steps involved

in generation of AHP ranking model. To validate the performance of generated AHP ranking model, two blind tests were performed independently. First test compared statistically significant amino acids of any randomly chosen thermophilic proteins and mesophilic proteins whereas, second test compared amino acids of any two randomly chosen mesophilic proteins from the existing dataset. These protein pairs were considered as alternatives for validation of generated AHP ranking model. The model assigned ranks to the comparing thermophilic and mesophilic protein pairs and classified as thermophilic or mesophilic. Thus, performance of the model was graded in terms of accuracy percentage enumerated using equation (1).

$$Accuracy\ \% = \frac{TP+TN}{TP+TN+FP+FN} \times 100 \quad (1)$$

TP (true positive), number of thermophilic proteins correctly classified as thermophilic proteins and TN (true negative), number of mesophilic proteins correctly classified as mesophilic proteins whereas, FP (false positive), number of mesophilic proteins incorrectly classified as thermophilic proteins and FN (false negative), number of thermophilic proteins incorrectly classified as mesophilic proteins.

2.5 *In silico* prediction of thermostabilizing mutations and their validation

According to the amino acid priorities in the relative abundance and ranking model, the thermostabilizing mutations were predicted in mesostable model enzyme *Bacillus subtilis* lipase with optimum stability at 35°C and pH 8 [21]. The structure of mutant lipases were modeled through I-TASSER server and the stability of the selected point mutation was confirmed through various prediction tools (such as I-Mutant 2.0, Cupsat, HotSpot Wizard, ERIS, etc.). The mutants were further validated through Ramachandran plot analysis (PROCHECK), structural superimposition analysis (PyMol V0.99), docking analysis using *p*-nitrophenol octanoate (*p*-NPO) substrate (Autodock 4.2 version) and contact map analysis (CMView 1.1.1).

2.6 Cloning, mutagenesis, overexpression and purification of lipase

Bacillus subtilis 168 lipase was cloned in pET-28a (+) using BamHI and NdeI restrictions sites. The site directed mutagenesis was carried out for attaining thermostability through designed mutagenic primers (Table S2) using QuikChange® Multi Site-Directed Mutagenesis Kit (Agilent Genomics) as per manufacturer's protocol. The selected thermostabilizing mutations were derived as per the *in silico* analysis. The cloning and mutations of lipases was confirmed through restriction digestion and sequence analysis.

For overexpression and purification, the recombinant plasmids of wild-type and mutant lipases were transformed into competent *E. coli* BL21 (DE3). The induced cultured cells (100 µM IPTG) were harvested by centrifugation (7000 ×g, 4°C, 10 min) followed by lysis in 10 mL phosphate buffer (20 mM, pH 8) containing 0.5 mg mL^{-1} of lysozyme. The suspended cells were sonicated to recover the soluble enzymes by centrifugation (14000 × g, 4°C, 20 min). N-terminal poly-histidine tag was used for purification of recombinant lipases using Ni-NTA affinity chromatography. Purified lipases were eluted by same buffer containing 250 mM imidazole. The purification of lipases was confirmed by SDS-PAGE (Bio-Rad laboratories) [22]. The free imidazole in the purified lipases was removed by dialysis in the same buffer at 4°C, followed by determination of concentrations of lipases by Bradford assay using BSA as standard (Fig. S2) [23].

2.7 Lipase activity assay

Activity of wild-type and mutant lipases were determined spectrophotometrically (UV-2600, Shimadzu) using *p*-NPO as substrate [24]. The amount of released *p*-nitrophenol (*p*-NP, $\varepsilon = 15.1$ mM cm^{-1}) was measured at 410 nm. One enzyme unit (U) was defined as the lipase activity that liberated 1 µmol equivalent of *p*-NP mL^{-1} min^{-1} under the standard assay conditions. The enzyme

kinetic parameter such as activity, specific activity, K_m value, turnover number (k_{cat}) and catalytic efficiency (k_{cat}/K_m) was calculated for wild-type and mutant lipases.

2.8 Characterization of wild-type and mutant lipases

Optimum temperature and pH of wild-type and mutant lipases was determined by incubating them with *p*-NPO for 10 min at varying range of temperatures (20 °C to 70 °C) and pH (pH 3 to pH 12), respectively. The temperature and pH stability of lipases were performed at thermal temperature of 55 °C and alkaline pH 9 at varying time intervals for 24 h. For melting temperature (T_m) determination of lipases, differential scanning fluorimetry (DSF) was performed using real-time PCR (Agilent Technologies) as reported earlier [22]. The reaction mixtures containing 0.1 mg mL^{-1} lipase and 5X SYPRO orange were placed in real-time PCR and set the temperature scan from 25 to 95 ºC, at 1 ºC min^{-1} ramp rate. The fluorescence of SYPRO orange dye (excitation maxima at 492 nm and emission maxima at 610 nm) was measured to determine the T_m of the lipases.

2.9 Determination of secondary structure changes of lipases by ATR-FTIR

Changes in secondary structures of lipases were investigated by FT-IR (Perkin-Elmer) in attenuated total reflection (ATR) mode in the range of amide I (1600-1700 cm^{-1}). Before recording the spectra, the lipase preparations were desalted by dialysis and dried at 37 °C. Peak positions in amide I range were resolved and fitted with a Gaussian shape using second derivative (OriginPro 8.5 software).

2.10 Determination of lipase compatibility with surfactants, oxidizing agents and commercial detergents

The compatibility of wild-type and mutant lipases with various surfactants (10 % v/v or w/v), oxidizing agents (1 % v/v or w/v) and commercial detergents (10 % v/v or w/v) was investigated

by incubating the lipase (50 U mL^{-1}) for 1 h at 35 °C. For commercial detergents, the endogenous lipases present were inactivated by heating the diluted detergents at 90 °C for 1 h prior to the addition of lipase preparation. Finally, the relative activity of wild-type and mutant lipases was determined and compared with control (having wild-type lipase but without any surfactants, oxidizing agents and commercial detergents). The detergent compatible lipases was chosen and subjected for immobilization on ZnO nanoparticles.

2.11 Covalent immobilization of lipase on synthesized ZnO nanoparticles

ZnO nanoparticles were synthesized by direct precipitation method using $ZnSO_4$ and NaOH as per Patel et al. (2016) [25]. The covalent immobilization procedure was developed using mild glutaraldehyde (GLU) as cross-linking agent for immobilization of lipases on functionalized ZnO nanoparticles (*i.e.* ZnO-PEI-APTES) via NH_2-groups. Glutaraldehyde is a powerful and versatile cross-linker in enzyme immobilization due its polymeric conformations which are formed depending on the reaction condition pH, temperature, concentration, etc. and can react with various groups other than amines such as, imidazoles, thiols, phenols etc. [15,16]. It has been found to be an effective way to attain improved activity and stability of lipases [26,27]. Briefly, 10 mg of functionalized ZnO-PEI/APTES was incubated in 10 mL phosphate buffer solution (20 mM, pH 8.0) containing 0.25 % (w/v) GLU and allowed to react for 2 h under stirring (100 rpm) at room temperature. Then, 1 mL of lipase solution (10 mg mL^{-1}) was added into the mixture and stirred for 2 h. The stepwise protocol of synthesis, functionalization and immobilization have been illustrated in Fig. 1.

2.12 Characterization of as-synthesized and lipase immobilized ZnO nanoparticles

Structure and morphology of naïve and bioconjugated ZnO nanoparticles was characterized by FESEM (Zeiss, Sigma, Germany) and TEM (JEM – 2100 HRTEM, JEOL, Japan). The particle

size was determined by dynamic light scattering (DLS; Beckmen Coulter Inc.). The optical absorption property of ZnO was studied by UV–vis spectroscopy (Shimadzu Corporation, Japan) in the range of 200 to 700 nm. FT-IR spectrometer (Perkin-Elmer, USA) was used to record spectra from 400 cm^{-1} to 4000 cm^{-1} at 4 cm^{-1} resolution with an average of 20 scans. The crystallinity of ZnO nanoparticles was determined using X-ray diffractometer (XRD; Rigaku TTRAX, Seifert XRD 3003 T/T) equipped with a Cu Kα radiation (K=1.54 Å) source, maintaining applied voltage of 40 kV and current at 30 mA. XRD analysis of the ZnO nanoparticles was performed in the 2θ range of 25° - 70° with speed of 5.0° as X-ray pattern of ZnO samples can be determined by varying angle (??) of incident X-ray beam that transits from constructive to destructive interference and referred as the function of X-ray angle *i.e.* 2??.

2.13 Estimation of immobilization efficiency and yield

Lipase immobilization efficiency and yield was estimated by Bradford assay and was calculated by equation (2) and (3), respectively [28].

$$Efficiency\ of\ immobilization\ (\%) = \frac{E_0 - E_1}{E_0} \times 100 \quad (2)$$

$$Immobilization\ yield\ (\%) = \frac{Y_1}{Y_0} \times 100 \quad (3)$$

E_0, amount of total protein introduced for immobilization; E_1, amount of protein present in the filtrate solutions after immobilization; Y_0, initial lipase activity for immobilization; and Y_1, activity immobilized lipase on the support. Further, optimum temperature and pH was determined for the immobilized enzymes.

2.14 Reusability and storage stability of immobilized lipases

In order to investigate the operational reusability, the immobilized lipase was separated by centrifugation, washed and eventually reused with fresh substrates for upto 20 cycles of experiment. The storage stability of the free and immobilized wild-type and mutant lipases was

investigated by calculating the residual activity till 60 days of experiment at regular intervals of 4 days.

2.15 Compatibility and washing performance of immobilized lipases

The immobilized wild-type and mutant lipases were again tested for surfactants, oxidizing agents and commercial detergents compatibility and further used for investigating washing performance [3]. Prior to soiling of cotton fabrics (4 cm^2) with olive oil and grease, defatting was performed in boiling choloroform. For selection of better or optimized washing conditions, the washing process was done at different washing temperatures (30 – 70 °C) and time intervals (10 – 70 min) using different concentrations of detergents (upto 9 % w/v) and lipases (upto 70 U mL^{-1}). Stained fabrics were incubated in different washing solutions in Erlenmeyer flasks. Then, the washed soiled fabric was rinsed with 100 mL distilled water for 2 min and air dried. The weight of the fabric was measured for each washing formulation before and after the wash. The percentage of oil and grease removal was calculated by using the following formula as shown in equation (4).

$$\%\ Oil\ or\ Grease\ Removal = \frac{W_3 - W_1}{W_2 - W_1} \times 100 \qquad (4)$$

W_1, weight of cloth before applying oil/grease (mg); W_2, weight of cloth after applying oil/grease (mg); and W_3, weight of cloth after total oil/grease removal (mg).

2.16 Statistical Analyses

All the data were reported as mean ± S.D. and performed in triplicates. GraphPad Prism (version 6) was used to analyze all the data for Analysis of Variance (ANOVA). The values of $p < 0.05$ were considered as statistically significant.

3. Results and Discussion

3.1 *In silico* analysis of amino acid attributes for prediction of thermostabilizing mutations

Amino acids in a protein sequence plays pivotal role in attaining structural stability and increases the content of various non-covalent interactions. This have been considered as the major contributor for thermostability that makes the protein compact and rigid to sustain structural and functional integrity under elevated temperatures [29–31]. To understand the molecular basis of protein thermostability, a dataset was created containing 116 non-redundant and homologous thermophilic-mesophilic pairs. The mesophilic counterparts were chosen through BLASTp program with a threshold of ≥70% homology (Table S1). PEPSTATS server was used to enumerate percentage compositions of 29 amino acid features which included 20 standard amino acids (Ala, Arg, Asn, Asp, Cys, Gln, Glu, Gly, His, Ile, Leu, Lys, Met, Phe, Pro, Ser, Thr, Trp, Tyr and Val) and 9 amino acid classes (polar, Pol; non-polar, NPol; small, Sml; tiny, Tiny; aromatic, Aro; aliphatic, Ali; charged, Chrg; basic, Bsc; and acidic, Acd). Two-sample KS-test was further employed to filter the statistically significant amino acids in the comparing proteins. KS-test does not depend on cumulative distribution function of the comparing samples and adapted to give the correct *p*-values. It measured the statistically significant difference in the distribution of bipartite dataset on the basis of D-statistics which states the difference between empirical distribution functions of the two samples [32]. In the present study, KS-test showed that among 29 features, 19 amino acid features (Ala, Arg, Asn, Asp, Cys, Glu, Gln, His, Ile, Lys, Ser, The, Val, Acd, Bsc, Chrg, Pol, Sml and Tiny) were statistically significant. It showed that they were preferred either in thermophilic or mesophilic proteins. Similar analysis was carried out by Kumwenda et al. (2013) in homologous sequences of *Thermus scotoductus* and *Thermus thermophilus*. The amino acids were tested using *Student t*-test and *Wilcoxon t*-test in such sequences and showed increased substitution of charged amino acids (Arg and Glu) in *T. thermophilus* HB27 [33].

Next, to understand the importance of each amino acid contributing to protein thermostability, the relative abundance and ranking analysis were employed. Relative abundance was derived by calculating the weighted arithmetic mean difference of the same amino acid of thermophilic proteins and its mesophilic counterpart.[20] Results showed that the relative abundance of an amino acid can be either positive or negative. The positive relative abundance of an amino acid showed its preference for thermophilic proteins and negative relative abundance of an amino acid showed its preference for mesophilic proteins (Fig. 2A). The charged amino acid features (Chrg > Glu > Acd > Bsc > Arg > Lys) had higher abundance whereas, small and tiny amino acid features (Sml > Tiny > Gln > Ser > Thr > Ala > Asn > Pol) had lower abundance in thermophilic proteins. These preferences showed inverse trend in mesophilic proteins. Haney et al. (1999) depicted lower content of small/tiny uncharged polar residues (Ser, Asn, and Gln) and higher percentage of charged amino acids (Glu, Arg and Lys) in proteins of thermophilic *Methanococcus* species [34]. The positive contribution of charged amino acids are involved in ionic interaction and salt bridge formation for higher capacity to bind surface water molecules [30]. Earlier in 1998, Scandurra et al. reported charged amino acids play a significant role in protein thermostability and their higher contents make the protein robust [35]. Chan et al. (2011) reported that the charged amino acids are accumulated in thermophilic proteins in order to stabilize the surface exposed structures. Such amino acids form salt-bridges and ion-pairing for improved thermostability [36]. Contrarily, the small and tiny amino acids tend to impair ionic and hydrophobic interactions of secondary structures in thermophilic proteins [37]. It was also found that substitution of serine with bulky and charged residues increased protein thermostability [33]. Mizuguchi et al. (2007) corroborated these results and revealed substituting small uncharged amino acids (such as Gln and Ser) with charged amino acids (Glu, Arg and Lys)

enhanced protein thermostability [38]. Thus, amino acids substituted with charged amino acids enhance the non-covalent interactions to stabilize the structures under higher temperature.

To comprehend the order of amino acid preference for thermostability, AHP was employed that uses multi-criteria decision-making platform [39]. Here, AHP helps in prioritizing amino acid attributes which are contributing to thermostability as it assumes mutations and their selection parameters are empirical and balances the protein's biophysical pleiotropy under various selection pressures [40]. Though the other most commonly used method for rational designing is B-Factor-directed mutagenesis, it has been used to enhance thermostability of many enzymes through substitution of rigidifying residues at the mutagenic hotspots with increased B-value in their three-dimensional structures [41]. However, the advantage of AHP method is that it arrives at an empirical rule to rationalize the approach for engineering mutations *in vitro*. This was carried out by creation of a dataset of homologous thermophilic protein and mesophilic counterparts, prioritizing the multiple amino acid attributes leading to protein thermostability and development of a ranking model thereafter. The generated ranking model was trained by enumerating the priorities (or ranks) of differentiating amino acid attributes, and used these values to predict thermostabilizing mutations.

The priorities of amino acids for thermostability were predicted by calculating eigenvectors from the generated reciprocal pairwise comparison matrix (Table S3). According to Saaty (2008), the derived ranks can only be accepted as consistent if the consistency ratio (CR) of comparison matrix is less than 0.1 [39]. In the present analysis, CR was found to be 0.0013, indicating it to be consistent. This was followed by generation of ranking model that prioritized the amino acids for thermostability. It showed a trend of Glu > Arg > (Lys, Chrg, Bsc, Acd) > (Ile, Val) > Pol > (Ala, Asp, Tiny, Sml) > (His, Asn, Ser, Thr) > Cys > Gln (Fig. 2B). The results corroborated

with the relative abundance analysis and is in accordance with earlier reports [34,42]. It depicted that Glu had the highest priority followed by Arg and an equal contribution of Lys, charged, basic and acidic amino acids whereas, Gln was the least preferred. De Farias and Bonato (2003) found an interesting rule that the (Glu+Lys)/(Gln+His) ratio can differentiate between hyperthermophilic proteins (>4.5), thermophilic proteins (3.2–4.6) and mesophilic proteins (<2.5). This substantiated the present result where Glu and Lys (as in numerator) had higher priorities for hyperthermophiles/thermophiles than Gln and His (as in denominator). At higher temperatures, protein destabilization occurs due to the presence of thermolabile residues such as Asn and Gln that are prone to deamidation and Cys that leads to oxidation and β-elimination [43].

The performance of generated AHP ranking model was validated through two independent blind tests for predicting thermostabilizing mutations. The comparing proteins in both the blind tests were assigned ranks from which mean ranks were calculated. Results showed higher mean rank value of thermophilic proteins as they had large contents of amino acids having higher priority values. So, the rank difference of thermophilic and mesophilic proteins in the first blind test was higher than that of second blind test that compared mesophilic-mesophilic parts (Table 1). Thus, the performance accuracy of ranking model was calculated by first blind test and it was found to be 96.0 %. Therefore, this ranking model could easily differentiate the thermophilic-mesophilic protein pairs as well as mesophilic-mesophilic protein pairs. The generated model could also empirically enumerate the weightage of individual point mutation for attaining protein thermostability. Thus, any mutation in a mesophilic protein which leads to a rank higher than 0.5 compared to its wild-type counterpart can be predicted to be thermostabilizing.

3.2 Prediction and validation of thermostabilizing mutations in a mesophilic enzyme

B. subtilis 168 lipase was chosen as a model mesophilic enzyme for prediction followed by validation of thermostabilizing mutations through AHP model. Its use for engineering has various advantages over other proteins such as (a) smaller molecular weight, (b) well characterized 3D structure (PDB ID: 1I6W), (c) typical α/β hydrolase fold, (d) lack of lid domain, disulfide bonds and metal coordination in its structure, and (e) has been previously studied for thermostabilization through different engineering approaches [44–46]. Various combinations of mutations were tested in the lipase to substitute existing amino acids (mutational hotspots) with those having higher order in the ranking model (Fig. 3A). They were designed at loop and surface exposed regions not affecting any stabilizing center region(s) and active site(s) of the enzyme. Three lipase mutants were chosen with substitution of Glu (E) and Lys (K) *viz.* bsl_the1 (V149K, Q150E; AHP rank, 0.021), bsl_the2 (F41K, W42E, V149K, Q150E; AHP rank, 0.043) and bsl_the3 (F41K, W42E, P119E, Q121K, V149K, Q150E; AHP rank, 0.062) (Fig. 3B). Previously, Ozawa et al. (2001) reported the replacement of residues with Lys (K) and Glu (E) that caused thermostabilization [47].

The mutant enzymes were modeled using I-TASSER server. The stability of modeled mutants were checked by various web servers such as HotSpot Wizard, I-Mutant2, Cupsat, iPTREE-STAB, WET-STAB and ERIS on the basis of ΔΔG value change in the mutant with respect to wild-type.[30] The stabilizing mutations showed increased protein stability of mutant as their $\Delta\Delta G > 0$ whereas, destabilizing mutations showed $\Delta\Delta G < 0$. Fig. 3C summarizes the stabilizing mutations (represented by S) and destabilizing mutations (represented by D).

The structural superimpositions were analyzed in terms of root mean square deviation (RMSD) [48]. Higher the RMSD value, more is the deviation of the mutated structure from its template. Structural superimpositions of generated lipase mutants was performed using PyMol V0.99

showing negligible changes in RMSD (bsl_the1, 0.225 Å; bsl_the2, 0.234 Å; and bsl_the3, 0.242 Å) and has been represented in Fig. 3D. Further, docking of wild-type and mutant lipases was performed using C8 (*p*-NPO) substrate in Autodock 4.2 version. The docking results indicated enhanced stability and better substrate binding capacity of the mutant lipases. The binding energy of substrate for each lipases was calculated which is the sum of intermolecular energy and torsional energy [49]. The mutant lipases had slightly less binding energy (bsl_the1, -6.11 kcal mol^{-1}; bsl_the2, -6.36 kcal mol^{-1}; and bsl_the3, -7.61 kcal mol^{-1}) than that of the native wild-type (bsl_wt, -5.99 kcal mol^{-1}). The lower binding energy of mutants depicted stable lipase mutants and thus, the binding pocket of mutants were found to be intact [49]. Massive decrease in inhibition constant (kI) was observed indicating higher potential of substrate for binding with mutant lipases (Fig. 3E).

The rotations of the polypeptide backbone of wild-type and mutant lipases around their bonds between N-C_α (φ) and C_α-C (ψ) was determined by Ramachandran plot analysis. To validate the backbone structure of lipase variants, Ramachandran plots were generated using PROCHECK server. Fig. 3F represents the generated Ramachandran plot for wild-type and mutant lipases and summarizes the percentage of residues in the allowed (favoured) region. Mutation increased the percentage of residues in the favoured region implying the stable conformation of the mutants. Finally, contact map analysis revealed increase in the number of unique contacts in all mutant lipases (Fig. 3G). The increased in new contacts (interactions) formed were more than the number of contacts lost in the mutant lipases suggesting that the increased contacts may have induced compactness in the enzyme. The increase contacts are the characteristics of thermostable proteins since they induces compactness [50]. Thus, the generated lipase mutants have high probability of being thermostable.

3.3 Recombinant production and kinetic studies of wild-type and mutant lipases

The wild-type lipase (bsl_wt) was successfully cloned into pET28a vector followed by designing of chosen mutations in bsl_the1, bsl_the2 and bsl_the3. The mutations were carried out at V149K, Q150E in bsl_the1; F41K, W42E, V149K, Q150E in bsl_the2; and F41K, W42E, P119E, Q121K, V149K, Q150E in bsl_the3. The clones were confirmed through restriction digestion analysis (Fig. S3A) and mutations by sequencing. The cloned lipase variants were overexpressed, purified and resolved on SDS-PAGE which confirmed molecular weight at 19.4 kDa (Fig. S3B) [21]. The concentrations of purified lipases were 3.4 g L^{-1} for bsl_wt, 3.6 g L^{-1} for bsl_the1, 3.2 g L^{-1} for bsl_the2 and 3.5 g L^{-1} for bsl_the3. Further, kinetic parameters of lipase variants were determined from Michaelis-Menten and Lineweaver-Burk plots (Fig. S4). These studies revealed 1.5 fold increase in the activity of bsl_the3 followed by 1.2 fold in bsl_the2 and 1.1 fold in bsl_the1 compared to bsl_wt. The lipase mutants also showed increased turnover number as well as improved catalytic efficiency than of bsl_wt (Table 2).

3.4 Effect of temperature and pH on activity and stability of lipases

The effect of temperature on wild-type and mutant lipases were determined in terms of thermal activity and stability (Fig. 4A and 4B). The optimum enzyme activity of bsl_wt was obtained maximum at 35 °C which was maximally increased to 55 °C in bsl_the3 followed by 50 °C for bsl_the2 and 40 °C for bsl_the1. Previously, a thermostable mutant of *Bacillus subtilis* lipase (PDB ID: 3D2C) was obtained with 9 mutations by directed evolution strategies that showed optimum activity at 55 °C.[10] However, the optimum activity of 55 °C was achieved in mutant bsl_the3 by only 6 mutations using present approach of pre-predicted protein engineering. Further, all the three mutants and wild-type lipases were exploited for thermal stability analysis. The mutant bsl_the3 showed thermal tolerance *i.e.* retained 70 % of its activity after an

incubation period of 24 h, bsl_the2 retained around 50 % activity, bsl_the1 and bsl_wt retained < 30 % activity.

The change in pH affects the enzyme structure and thus, stability as well as activity [51]. The effect of different pH (at 35 °C) on activity and stability of lipases were determined (Fig. 4C and 4D). The optimum activity of bsl_wt was obtained at pH 8 that increased to pH 9 in bsl_the2 and bsl_the3 and pH 8.5 in bsl_the1. The mutants slightly shifted their optimum activity towards alkaline pH. Thus, the pH 9.0 was chosen for studying alkalistability of the lipases. The maximum relative activity was retained around 65 % for bsl_the3 and 50 % for bsl_the2 incubating at pH 9.0 for 24 h. However, the bsl_the1 and bsl_wt retained activity to < 30 %. Thus, the analysis of pH stability showed alkaline tolerance with retained activity for all the mutant variants.

Thermal shift assay was carried out through differential scanning fluorimetry and employed to monitor the temperature at which a protein unfolds *i.e.* melting temperature (T_m) of the enzyme [52]. The thermal profiles of mutant lipases showed thermal shift as bsl_the3 mutant showed highest increase in the T_m to 66.0 °C from 59.0 °C (bsl_wt) (Fig. 4E). The bsl_the1 (T_m = 60.5 °C) and bsl_the2 (T_m = 63.0 °C) also showed increase in their T_m. The predicted mutations resulted in increased thermal tolerance leading to structural rigidity. Song et al. (2000) and Kuo et al. (2017) independently showed that the thermostability and catalytic activity can be improved through evolutionary molecular engineering by a significant increase in the T_m of mutant enzyme [53,54].

3.5 Determination of secondary structural changes in mutant lipases

In protein infrared spectrum, the amide vibrations (A, B, I to VII) were determined for the presence of peptide groups. Amide I band (1600-1700 cm^{-1}) is mainly associated with C=O

stretching in the peptide bond and modulated by the protein secondary structure. In the present study, the amide I range in the FTIR spectrum of lipases were fitted with Gaussian curves and the content of secondary structures such as α-helix, β-sheet, β-turn, random coil were determined (Table 3 and Fig. S5). Peak for α-helix was found around 1655 cm^{-1}, β-sheet in 1620-1636 cm^{-1}, β-turn in 1662-1688 cm^{-1} and random coil at 1645 cm^{-1}. However, the reported crystal structure of *B. subtilis* lipase showed 46.93 % α-helix, 21.79 % β-sheets, 19.55 % turns and 11.73 % random coil (PDB ID: 1I6W). These values differed in mutant lipases and showed increase in α-helix and β-sheet by reducing the random coil that makes the lipase rigid and stable. The bsl_the2 and bsl_the3 showed higher percentage of α-helix and β-sheet. It is attributed to the increased hydrogen bonding between amine and carboxylic groups of the mutant lipases and contribute to make their structures robust after mutagenesis [55].

3.6 Screening of detergent compatible lipases

Lipase is an effective enzyme used to remove oily and greasy stains from the fabrics. Thus, they should be tolerant to harsh detergent industry conditions [56]. The wild-type and mutant lipases were incubated with various surfactants, oxidizing agents and commercial detergents and then assayed under standard conditions (Fig. 5). Comparative analysis revealed bsl_the3 was the most compatible lipase with various surfactants, oxidizing agents and commercial detergents. The highest relative activity (%) of 100.9 ± 2.7, 113.0 ± 2.0 and 101.0 ± 1.6 was obtained with Triton-X 100, NaClO and Ariel, respectively. Further, to improve the stability of lipases (the bsl_the3 and bsl_wt as control), immobilization was carried out on synthesized ZnO nanoparticles as they are cost-effective, biocompatible, non-toxic and environmental friendly. Previously it was reported that ZnO nanoparticles have compatibility with textile fabrics as they are UV-blocking, self-cleaning and have anti-bacterial properties [57]. This suggests that the use

of lipase immobilized ZnO nanoparticles in laundry detergent formulation for removal of stains from fabrics can be a promising approach.

3.7 Characterization of the as-synthesized and lipase immobilized ZnO nanoparticles

The most prevailing strategies of enzyme stabilization for any commercial application requires coupling of site-directed mutagenesis and chemical modification mediated enzyme immobilization [58]. The present study also aimed at immobilizing the engineered lipases on chemically modified ZnO nanoparticles with GLU, PEI and APTES to further improve their catalytic performance, storage stability and reusability. ZnO nanoparticles was synthesized using $ZnSO_4$ as precursor and immobilized with bsl_wt and bsl_the3. Their morphologies were characterized through FESEM (at 100 nm) and TEM (at 20 nm) analysis (Fig. 6A-F). The analyses showed flower or star-like morphology with multi-pod structures that consisted of 4-6 pod-like structures attached together in the center of ZnO crystal seed with the sharp part at the end of the branches. TEM analysis showed highly dense ZnO nanoparticles due to the increase in the concentration of precursor thereby increasing the growth and density of ZnO nanoparticles [59]. From the morphological data, it can be inferred that it may be due to Ostwald ripening phenomenon that the small crystals dissolved and deposited on larger particles surface leading to lower energy levels. The crystallization of the star-like structures may be due to (i) joining of the nuclei and generation of the symmetrical form in the primary steps of the growth process; (ii) agglomeration of the grown particles and formation of the ordered structure in the next steps of the crystallization; and (iii) alignment of the particles creating the flake-like pieces through the particle coalescence. Similar morphology of ZnO nanoparticles was previously reported in many literatures and these patterns exists due to the more stability in symmetric configurations [60,61]. Further, laser diffraction determined the particle hydrodynamic diameter and the particle size

distribution of as-synthesized and lipase immobilized ZnO nanoparticles in the suspension (Fig. 6G-I). The average hydrodynamic diameter of the as-synthesized ZnO nanoparticles was 157.4±8.5 nm with polydispersity index (PdI) of 0.176. The analyzed size of nanoparticles was based on their lengths [62]. It is in close agreement with earlier literature [63,64]. In TEM micrographs, the presence of nanoparticle aggregates could be clearly observed, which further supports the larger hydrodynamic diameter obtained from DLS [65,66].

The morphology and size distribution of bsl_wt and bsl_the3 immobilized ZnO nanoparticles were also studied using FESEM, TEM and DLS. The functionalized ZnO nanoparticles carries free NH_2-groups at their surfaces due to coating of PEI and APTES which was exploited for covalent immobilization of lipases via their surface NH_2-groups (Lys and Arg) using glutaraldehyde as cross-linking agent. This immobilization strategy is very versatile and rapid as glutaraldehyde utilizes NH_2-groups of PEI and APTES present on functionalized ZnO nanoparticles at low ionic strength which can cause effective covalent immobilization of lipases on the NH_2-active support through equilibrium shift [67]. In fact, glutaraldehyde are the small molecules which can cause effective intermolecular cross-linking of lipases with the NH_2-active support if increased lipase concentration is provided. This can lead to increased immobilization rate, activity and stability of lipases [27]. The possible mechanism behind the crosslinking of lipase and NH_2-active support via glutaraldehyde under alkaline conditions is through the formation of Schiff base linkages. This results into the formation of C–N bond between glutaraldehyde and amino groups of lipases or NH_2-active support through Michael addition [17]. The analysis in the present work showed lipase immobilization on to the as-synthesized ZnO nanoparticles that was clearly visible as the traces of protein deposited on their surfaces.

However, occasionally, the immobilized enzyme shows reduced stability, conformational change, inactivation and aggregations due to changes in the surrounding microenvironment and extent of multipoint attachment [68]. Thus, in such cases, for instance in lipases, the better efficiency after immobilization can be achieved by low ionic strength environments that reduces the lipase aggregation and cause multipoint immobilization through hydrophobic surfaces surrounding their catalytic site, as their activity greatly increases at the lipid-water interface by a phenomenon called interfacial activation. Recently, Arana-Peña et al. (2019) developed a novel strategy to reuse the most stable lipase by co-immobilizing different lipases on glyoxyl-octyl agarose via interfacial activation [69].

Upon covalent binding of the enzyme, the size and shape of the nanoparticles almost remained unchanged. It was observed that the surface of the nanoparticles was porous in nature. The pores and cracks may be attributed to the agglomeration of nanoparticles on the surface as reported earlier [25,70]; DLS analysis showed average size of 208.0±6.1 nm (PdI = 0.221) in ZnO-bsl_wt and 238.6±6.9 nm (PdI = 0.252) in ZnO-bsl_the3. The increase in the average size of as-synthesized ZnO revealed lipases were successfully immobilized on the nanoparticles. Next, from the diffraction rings of SAED pattern (inset of Fig. 6D-F), concentric rings indicated highly crystalline nature as well as (101) and (103) planes of the ZnO nanoparticles were identified which is in good agreement with the XRD results discussed in the proceeding section.

The optical property of the as-synthesized and lipase immobilized ZnO nanoparticles was examined through UV-Vis spectroscopy (Fig. 7A). The as-synthesized ZnO nanoparticles maximally absorbed the UV radiations at 372 nm and almost all the visible spectrum radiations were transmitted. The optical band gap energy has been calculated by $E(eV) = 1.2398/\lambda(\mu m)$ and was found to be 3.33 eV. The ZnO-bsl_wt and ZnO-bsl_the3 exhibited an additional protein

characteristics absorbance peak at ~280 nm (aromatic ring of amino acids) and ~220 nm (peptide bonds) with a featured characteristic peak of ZnO at 375 nm and 377 nm. This confirmed the immobilization of bsl_wt and bsl_the3 on to the ZnO nanoparticles [71]. The calculated band gap energy was 3.30 eV for ZnO-bsl_wt and 3.29 eV for ZnO-bsl_the3. Thus, slight red shift behaviour in the band gap was observed upon lipase immobilization. It leads to quenching the electrons in the conduction band in case of lipase immobilized ZnO nanoparticles [72]. While some authors reported blue shifting due to unfavorable interactions of dipole moments of polar solvent molecules with fluorophores of enzyme under excited state [70], others have observed red shifts due to the reduced nature of enzymes which resulted in the reduction of surface states (pre-adsorbed oxygen) of the ZnO nanoparticles [73],

The synthesis and immobilization of ZnO nanoparticles was also investigated by FTIR analysis (Fig. 7B). The FTIR spectra indicated the typical ZnO peaks beyond 600 cm^{-1} in both as-synthesized and lipase immobilized ZnO nanoparticles suggesting the presence of ZnO material.[28] The stretching peak of -OH groups was noticed around 3600 - 3200 cm^{-1} indicating their presence of water molecules on the surface of ZnO nanoparticles. The ZnO-PEI showed strong twin peaks at 1636 and 1044 cm^{-1} and a broad peak in the 3200 - 3450 cm^{-1} region. The glutaraldehyde-activated ZnO-PEI-APTES showed peaks in 1035 - 1050 cm^{-1} which could be assigned to Si-O stretching vibration.[70] Most characteristic bands ranging from 1350 - 1750 cm^{-1} were associated in ZnO immobilized lipases which were due to amide bonds (C-N, C=O and N-H groups) in the protein. This range mainly comprised of amide I (stretching vibration of C=O), amide II and amide III (both associated with coupled C–N stretching and N–H bending vibrations of the peptide group) that are the main signal for the identification of protein secondary structures [28]. The peaks of amide bonds reflect the structure of the main polypeptide

chain irrespective of side groups. The amide bond linking the PEI generally comes in the near region of 1600 cm^{-1}. In the present spectra, it was overlapped with the N-H bending mode of ZnO immobilized lipases. The peaks from 1500 to 1700 cm^{-1} and 2500 to 2900 cm^{-1} represents the functional groups corresponding to C-O stretching and C-H stretching mode, respectively. These additional peaks were further specific to nanoparticle functionalization and lipase immobilization.

According to the XRD spectrogram of the as-synthesized ZnO, the well-defined peaks of typical ZnO was clearly noticed (Fig. 7C). The as-synthesized ZnO showed the diffraction peaks located at 31.84°, 34.52°, 36.33°, 47.63°, 56.71°, 62.96°, 68.13°, and 69.18°. All the peaks of XRD were matched with the wurtzite phase of ZnO by comparison with the data from reports on powder diffraction standard ICDD card number 98-010-8249 [74]. The particle size was computed using Debye-Scherrer formula ($D = 0.9\lambda / \beta \cos \theta$) and the FWHM (full width at half maximum) value corresponding to the major plane (101), was ~18 nm. Interestingly, lipase immobilized ZnO nanoparticles showed peaks at same locations but their intensity decreased significantly due to loss of crystalline structure of ZnO nanoparticles after immobilization. Also, the XRD pattern for as-synthesized ZnO nanoparticles showed much sharper peaks indicating more crystalline nature of than ZnO-bsl_wt and ZnO-bsl_the3. Peak broadening of lipase immobilized ZnO nanoparticles indicated a lattice distortion due to the enzyme introduction. Increase in the intensity of (002) peak upon enzyme loading further suggested preferred unidirectional growth. The compactness and clear resolution of the peaks towards lower angles suggested ordered and compact enzyme layer on the surface of nanoparticles [70].

3.10 Kinetic and physicochemical parameters of ZnO immobilized lipases

The kinetics and physicochemical parameters of immobilized enzymes are influenced by the carrier material [75]. Thus, factors like immobilization efficiency, immobilization yield, optimum activity, etc. were determined for ZnO-bsl_wt and ZnO-bsl_the3 (Table 4). ZnO-bsl_wt and ZnO-bsl_the3 showed immobilization efficiency of 82.5 % and 88.5 %, respectively. The lipase activity of immobilized enzymes were estimated by calculating immobilization yield. It revealed that 71.9 % activity was retained in ZnO-bsl_wt and 79.5 % in ZnO-bsl_the3. The decrease in the activity after immobilization may be contributed to the covalent binding of the lipases onto the ZnO nanoparticles [76]. Further, the optimum temperature and pH were investigated for immobilized lipases at various temperatures (10 °C to 70 °C) and pH (pH 3 to pH 12). Further, post immobilization, the ZnO-bsl_wt activity was enhanced to 40 °C, pH 8.5 and ZnO-bsl_the3 to 60 °C, pH 10. This covalent immobilization of lipases with ZnO nanoparticles also reduces conformational flexibility leading to higher activation energy for the enzymes to reorganize proper conformation of substrate binding site thereby enhancing activity under high temperature and pH [77].

3.11 Reuse and storage stability of ZnO immobilized lipases

The major limitations of enzymes in industrial process are their reusability in continuous reactions. The ZnO immobilized lipases can easily be separated from the reaction mixture through centrifugation and subsequently can be reused for hydrolysis of the substrate. The reusability of ZnO-bsl_wt and ZnO-bsl_the3 were assayed over 20 reaction cycles under optimized conditions. Relative activity of the first run was set to 100% and the retention activity for further reuses were determined (Fig. 8A). ZnO-bsl_wt and ZnO-bsl_the3 retained 38 % and 78 % of its initial activity after 20 cycles. The decrease in the activity of immobilized lipases after recycling was either due to weakening of binding strength between ZnO matrix and lipases

leading to enzyme leaching or the recurrent encountering of substrate with the active site of immobilized lipases causing distortion and loss of activity [78].

The storage stability of the free (bsl_wt and bsl_the3) and immobilized lipases (ZnO-bsl_wt and ZnO-bsl_the3) were determined at room temperature and their catalytic activities were evaluated till 60 days at an interval of 4 days. Both the immobilized lipases showed improved storage stability (Fig. 8B). ZnO-bsl_wt and ZnO-bsl_the3 retained 63 % and 80 % of its initial activity whereas the free lipases could retain less than 30% of the initial activity. Nevertheless, the immobilization analysis of ZnO-bsl_wt and ZnO-bsl_the3 did not show a large difference on storage stability but more in reusability. It may be due to early leaching of bsl_wt than bsl_the3 from the solid matrix during its reuse. This is because mutant lipase (bsl_the3) has three surface exposed Lys substitutions at F41, P119 and V149 which may be responsible for increased multipoint attachments of mutant with functionalized nanoparticles. However, immobilization significantly prevented enzyme deactivation and subsequently improved the storage stability as well as reusability of the mutant enzyme [79].

3.12 Compatibility of immobilized lipases as detergent additive for destaining of fabric

The ZnO-bsl_wt and ZnO-bsl_the3 were examined for compatibility with various surfactants, oxidizing agents and commercial detergents (Fig. 9A). The activity of ZnO-bsl_wt was considered as control (without any detergent additives) with 100 % activity. The relative activity of ZnO-bsl_the3 gave better performance with detergent additives and showed better compatibility with Ariel. Therefore, Ariel was used for oil and grease destaining experiments and its indigenous lipases was thermal deactivated prior to its use for destaining. Earlier reports showed that the removal of oily and greasy stains was enhanced using commercial detergent when used indigenously with lipase of *Pseudozyma* sp. NII 08165 and *Pseudomonas aeruginosa*

[80,81]. Further, the destaining of grease and oil stained fabrics was optimized for four parameters such as lipase concentration, detergent (Ariel) concentration, washing temperature and washing time using ZnO-bsl_wt and ZnO-bsl_the3 (Fig. 9B-I). In optimization of lipase concentrations, ZnO-bsl_wt and ZnO-bsl_the3 showed maximum oil and grease removal at 50 U mL^{-1}. ZnO-bsl_the3 had higher oil and grease removal upto 90 % and 82 %, respectively. The optimized detergent concentration for both the ZnO-bsl_wt and ZnO-bsl_the3 showed higher oil removal with 5 % Ariel and grease removal with 6 % Ariel from the fabric. The optimum washing temperature for efficient oil and grease removal showed highest temperature stability at 55 °C for ZnO-bsl_the3 whereas, 40 °C was suitable for ZnO-bsl_wt. Higher temperature is the prerequisite for better oil and grease removal from the fabrics [4,82]. Therefore, the thermotolerant ZnO-bsl_the3 gave higher oil and grease removal from the fabrics than ZnO-bsl_wt. The optimal washing time of ZnO-bsl_the3 for oil removal from the fabric was 30 min and grease removal was 40 min. These results corroborated with previous reports that showed stain removal is more in presence of lipases with increased washing time [80,81]. Washing solution containing only detergent (Ariel) served as control (except in optimization of lipase concentrations) and showed only 21 % and 17 % of oil and grease removal, respectively. In the optimized parameters, ZnO-bsl_the3 showed maximum oil and grease removal upto 90 % and 82 %, respectively whereas, ZnO-bsl_wt showed 62 % oil removal and 57 % grease removal. The photographs and FESEM micrographs showing destaining was carried out using ZnO-bsl_wt and ZnO-bsl_the3 at obtained optimized lipase concentration, detergent (Ariel) concentration, washing temperature and time are represented in Fig. 10.

4. Conclusion

The present research was an effort to decipher amino acid adaptations in thermophilic proteins to achieve thermal robustness. The contributing amino acids were analyzed and classified using relative abundance followed by ranking them for their contribution in thermophilic proteins. Analysis revealed priority of charged amino acids (such as Glu, Arg and Lys) for thermostability. These positively contributing attributes have been further exploited to design mutations in a mesophilic protein in such a way to increase the content of these attributes to endorse the prediction of generated models. The predicted mutations in *Bacillus subtilis* lipase (a chosen mesophilic enzyme) were validated through various *in silico* and experimental approaches. *In silico* validation showed the designed mutations were found to be stabilizing and did not affect the catalytic activity of the lipase. Experimentally, the mutant lipase (bsl_the3) showed enhanced optimum activity and stability maximally to thermal temperature 55 °C and alkaline pH 9. Rigidity of mutant lipases was improved by increasing in the percentage of helices and sheets that resulted into enhanced thermostability of lipases. The novelty lies in moving from random mutagenesis to a pre-predicted approach by ranking the contributing attributes rendering thermostability for a rationalized protein engineering platform.

The produced thermostable lipase mutants were subjected for enzymatic detergent formulations. To further increase the enzyme stability, engineered lipases were immobilized on synthesized ZnO nanoparticles as it is cheap, biocompatible and environmental friendly. The synthesized ZnO nanoparticles and lipase immobilization was confirmed using UV-Vis, FT-IR, DLS, powder XRD, TEM and FESEM analysis. Interestingly, ZnO immobilized engineered lipases further enhanced the enzyme activity (to 60 °C and pH 10), storage stability, reusability and their compatibility with various oxidizing agents, surfactants and commercial detergents. The immobilized biocatalysts were subjected for removal of oil and grease stains from cotton fabrics.

The destaining process was optimized at different temperatures and time intervals using different concentrations of detergent and lipase activities. Under optimized conditions, the maximum removal of oil and grease stains were upto 90 % and 82 %, respectively. Thus, the nanoparticle conjugated biocatalysts proved to be a promising approach in detergent formulation which was produced through rationalized protein engineering approach.

Declaration of interest

Authors have no conflict of interest.

Acknowledgements

Wild-type lipase cloned pET-21b vector was a kind gift from Dr. N. Madhusudhan Rao of Centre for Cellular & Molecular Biology (CCMB), India. MFK acknowledges Indian Institute of Technology Guwahati for providing PhD research fellowship. DK and CH are grateful to Science and Engineering Research Board, Department of Science and Technology, New Delhi (File Number: PDF/2015/000382 and PDF/2015/000388) for National Post-Doctoral Fellowship (N-PDF).

References

[1] J. Adrio, A. Demain, Microbial enzymes: tools for biotechnological processes, Biomolecules. 4 (2014) 117–139. https://doi.org/10.3390/biom4010117.

[2] J.M. Choi, S.S. Han, H.S. Kim, Industrial applications of enzyme biocatalysis: Current status and future aspects, Biotechnol. Adv. 33 (2015) 1443–1454. https://doi.org/10.1016/j.biotechadv.2015.02.014.

[3] M. Chauhan, R.S. Chauhan, V.K. Garlapati, Evaluation of a new lipase from *Staphylococcus* sp. for detergent additive capability, Biomed Res. Int. 2013 (2013) 374967. https://doi.org/10.1155/2013/374967.

[4] H. Horchani, H. Mosbah, N. Ben Salem, Y. Gargouri, A. Sayari, Biochemical and molecular characterisation of a thermoactive, alkaline and detergent-stable lipase from a newly isolated *Staphylococcus aureus* strain, J. Mol. Catal. B Enzym. 56 (2009) 237–245. https://doi.org/10.1016/j.molcatb.2008.05.011.

[5] H. Yu, H. Huang, Engineering proteins for thermostability through rigidifying flexible sites, Biotechnol. Adv. 32 (2014) 308–315. https://doi.org/10.1016/j.biotechadv.2013.10.012.

[6] S. Lutz, Beyond directed evolution—semi-rational protein engineering and design, Curr. Opin. Biotechnol. 21 (2010) 734–743. https://doi.org/10.1016/j.copbio.2010.08.011.

[7] K.L. Schweiker, G.I. Makhatadze, Chapter 7 A computational approach for the rational design of stable proteins and enzymes, in: M.L. Johnson, L. Brand (Eds.), Methods Enzymol., Elsevier, 454 (2009), pp. 175–211. https://doi.org/10.1016/S0076-6879(08)03807-X.

[8] H. Yu, Y. Yan, C. Zhang, P.A. Dalby, Two strategies to engineer flexible loops for improved enzyme thermostability, Sci. Rep. 7 (2017) 41212. https://doi.org/10.1038/srep41212.

[9] K. Boonyapakron, A. Jaruwat, B. Liwnaree, T. Nimchua, V. Champreda, P. Chitnumsub, Structure-based protein engineering for thermostable and alkaliphilic enhancement of endo-β-1,4-xylanase for applications in pulp bleaching, J. Biotechnol. 259 (2017) 95–102. https://doi.org/10.1016/j.jbiotec.2017.07.035.

[10] S. Ahmad, M.Z. Kamal, R. Sankaranarayanan, N.M. Rao, Thermostable *Bacillus subtilis* lipases: in vitro evolution and structural insight, J. Mol. Biol. 381 (2008) 324–340. https://doi.org/10.1016/j.jmb.2008.05.063.

[11] M.J. Thompson, D. Eisenberg, Transproteomic evidence of a loop-deletion mechanism for enhancing protein thermostability, J. Mol. Biol. 290 (1999) 595–604. https://doi.org/10.1006/jmbi.1999.2889.

[12] C. Mateo, J.M. Palomo, G. Fernandez-Lorente, J.M. Guisan, R. Fernandez-Lafuente, Improvement of enzyme activity, stability and selectivity via immobilization techniques, Enzyme Microb. Technol. 40 (2007) 1451–1463. https://doi.org/10.1016/j.enzmictec.2007.01.018.

[13] L. Cao, Immobilised enzymes: science or art?, Curr. Opin. Chem. Biol. 9 (2005) 217–226. https://doi.org/10.1016/j.cbpa.2005.02.014.

[14] E.P. Cipolatti, A. Valerio, R.O. Henriques, D.E. Moritz, J.L. Ninow, D.M.G. Freire, E.A. Manoel, R. Fernandez-Lafuente, D. de Oliveira, Nanomaterials for biocatalyst immobilization–state of the art and future trends, RSC Adv. 6 (2016) 104675–104692. https://doi.org/10.1039/C6RA22047A.

[15] I. Migneault, C. Dartiguenave, M.J. Bertrand, K.C. Waldron, Glutaraldehyde: behavior in aqueous solution, reaction with proteins, and application to enzyme crosslinking, Biotechniques. 37 (2004) 790–802. https://doi.org/10.2144/04375RV01.

[16] O. Barbosa, C. Ortiz, Á. Berenguer-Murcia, R. Torres, R.C. Rodrigues, R. Fernandez-Lafuente, Glutaraldehyde in bio-catalysts design: A useful crosslinker and a versatile tool in enzyme immobilization, RSC Adv. 4 (2014) 1583–1600. https://doi.org/10.1039/C3RA45991H.

[17] Y. Wine, N. Cohen-Hadar, A. Freeman, F. Frolow, Elucidation of the mechanism and end products of glutaraldehyde crosslinking reaction by X-ray structure analysis, Biotechnol. Bioeng. 98 (2007) 711–718. https://doi.org/10.1002/bit.21459.

[18] R.C. Rodrigues, C. Ortiz, Á. Berenguer-Murcia, R. Torres, R. Fernandez-Lafuente, Modifying enzyme activity and selectivity by immobilization, Chem. Soc. Rev. 42 (2013) 6290–6307. https://doi.org/10.1039/C2CS35231A.

[19] G. Fernandez-Lorente, J.M. Palomo, C. Mateo, R. Munilla, C. Ortiz, Z. Cabrera, J.M. Guisán, R. Fernandez-Lafuente, Glutaraldehyde cross-linking of lipases adsorbed on aminated supports in the presence of detergents leads to improved performance, Biomacromolecules. 7 (2006) 2610–2615. https://doi.org/10.1021/bm060408+.

[20] M.F. Khan, S. Patra, Deciphering the rationale behind specific codon usage pattern in extremophiles, Sci. Rep. 8 (2018) 15548. https://doi.org/10.1038/s41598-018-33476-x.

[21] P. Acharya, E. Rajakumara, R. Sankaranarayanan, N.M. Rao, Structural Basis of Selection and Thermostability of Laboratory Evolved *Bacillus subtilis* Lipase, J. Mol. Biol. 341 (2004) 1271–1281. https://doi.org/10.1016/j.jmb.2004.06.059.

[22] P. Saha, M.F. Khan, S. Patra, Truncated α-amylase: an improved candidate for textile processing, Prep. Biochem. Biotechnol. 48 (2018) 635–645. https://doi.org/10.1080/10826068.2018.1479863.

[23] M.M. Bradford, A rapid and sensitive method for the quantitation of microgram quantities of protein utilizing the principle of protein-dye binding, Anal. Biochem. 72 (1976) 248–254. https://doi.org/10.1016/0003-2697(76)90527-3.

[24] A. Glogauer, V.P. Martini, H. Faoro, G.H. Couto, M. Müller-Santos, R.A. Monteiro, D.A. Mitchell, E.M. de Souza, F.O. Pedrosa, N. Krieger, Identification and characterization of a new true lipase isolated through metagenomic approach, Microb. Cell Fact. 10 (2011) 54. https://doi.org/10.1186/1475-2859-10-54.

[25] V. Patel, C. Shah, M. Deshpande, D. Madamwar, Zinc oxide nanoparticles supported

lipase immobilization for biotransformation in organic solvents: a facile synthesis of geranyl acetate, effect of operative variables and kinetic study, Appl. Biochem. Biotechnol. 178 (2016) 1630–1651. https://doi.org/10.1007/s12010-015-1972-9.

[26] O. Barbosa, R. Torres, C. Ortiz, R. Fernandez-Lafuente, The slow-down of the CALB immobilization rate permits to control the inter and intra molecular modification produced by glutaraldehyde, Process Biochem. 47 (2012) 766–774. https://doi.org/10.1016/j.procbio.2012.02.009.

[27] R.C. Rodrigues, J.J. Virgen-Ortíz, J.C.S. dos Santos, Á. Berenguer-Murcia, A.R. Alcantara, O. Barbosa, C. Ortiz, R. Fernandez-Lafuente, Immobilization of lipases on hydrophobic supports: immobilization mechanism, advantages, problems, and solutions, Biotechnol. Adv. 2019. https://doi.org/10.1016/j.biotechadv.2019.04.003.

[28] S. Ghasemi, M. Heidary, M.A. Faramarzi, Z. Habibi, Immobilization of lipase on Fe3O4/ZnO core/shell magnetic nanoparticles and catalysis of Michael-type addition to chalcone derivatives, J. Mol. Catal. B Enzym. 100 (2014) 121–128. https://doi.org/10.1016/j.molcatb.2013.12.006.

[29] M. Ebrahimi, A. Lakizadeh, P. Agha-Golzadeh, E. Ebrahimie, M. Ebrahimi, Prediction of thermostability from amino acid attributes by combination of clustering with attribute weighting: a new vista in engineering enzymes, PLoS One. 6 (2011) e23146. https://doi.org/10.1371/journal.pone.0023146.

[30] D. Chakravorty, M.F. Khan, S. Patra, Multifactorial level of extremostability of proteins: can they be exploited for protein engineering?, Extremophiles. 21 (2017) 419–444. https://doi.org/10.1007/s00792-016-0908-9.

[31] D. Chakravorty, M.F. Khan, S. Patra, Thermostability of proteins revisited through

machine learning methodologies: from nucleotide sequence to structure, Curr. Biotechnol. 6 (2017) 39–49. https://doi.org/10.2174/2211550105666151222183232.

[32] T.J. Pasieka, R.F. Woolson, C. Grose, Viral induced fusion and syncytium formation: Measurement by the Kolmogorov-Smirnov statistical test, J. Virol. Methods. 111 (2003) 157–161. https://doi.org/10.1016/S0166-0934(03)00152-6.

[33] B. Kumwenda, D. Litthauer, O.T. Bishop, O. Reva, Analysis of protein thermostability enhancing factors in industrially important thermus bacteria species, Evol. Bioinform. 9 (2013) 327–42. https://doi.org/10.4137/EBO.S12539.

[34] P.J. Haney, J.H. Badger, G.L. Buldak, C.I. Reich, C.R. Woese, G.J. Olsen, Thermal adaptation analyzed by comparison of protein sequences from mesophilic and extremely thermophilic *Methanococcus* species, Proc. Natl. Acad. Sci. U. S. A. 96 (1999) 3578–3583. https://doi.org/10.1073/pnas.96.7.3578.

[35] R. Scandurra, V. Consalvi, R. Chiaraluce, L. Politi, P.C. Engel, Protein thermostability in extremophiles, Biochimie. 80 (1998) 933–941. https://doi.org/10.1016/S0300-9084(00)88890-2.

[36] C.H. Chan, T.H. Yu, K.B. Wong, Stabilizing salt-bridge enhances protein thermostability by reducing the heat capacity change of unfolding, PLoS One. 6 (2011) e21624. https://doi.org/10.1371/journal.pone.0021624.

[37] L. Sawle, K. Ghosh, How do thermophilic proteins and proteomes withstand high temperature?, Biophys. J. 101 (2011) 217–227. https://doi.org/10.1016/j.bpj.2011.05.059.

[38] K. Mizuguchi, M. Sele, M.V. Cubellis, Environment specific substitution tables for thermophilic proteins, BMC Bioinformatics. 8 (2007) S15. https://doi.org/10.1186/1471-2105-8-S1-S15.

[39] K. Peniwati, Group decision making: drawing out and reconciling differences, Int. J. Anal. Hierarchy Process. 9 (2017). https://doi.org/10.13033/ijahp.v9i3.533.

[40] S. Murakami, H. Oshima, T. Hayashi, M. Kinoshita, On the physics of thermal-stability changes upon mutations of a protein, J. Chem. Phys. 143 (2015) 09B619_1. https://doi.org/10.1063/1.4931814.

[41] X. Duan, S. Cheng, Y. Ai, J. Wu, Enhancing the thermostability of *Serratia plymuthica* sucrose isomerase using B-factor-directed mutagenesis, PLoS One. 11 (2016) e0149208. https://doi.org/10.1371/journal.pone.0149208.

[42] V. Parthiban, M.M. Gromiha, D. Schomburg, CUPSAT: prediction of protein stability upon point mutations, Nucleic Acids Res. 34 (2006) W239-W242. https://doi.org/10.1093/nar/gkl190.

[43] S. Kumar, C.J. Tsai, R. Nussinov, Factors enhancing protein thermostability, Protein Eng. Des. Sel. 13 (2000) 179–191. https://doi.org/10.1093/protein/13.3.179.

[44] F.I. Khan, D. Lan, R. Durrani, W. Huan, Z. Zhao, Y. Wang, The lid domain in lipases: Structural and functional determinant of enzymatic properties, Front. Bioeng. Biotechnol. 5 (2017) 16. https://doi.org/10.3389/fbioe.2017.00016.

[45] G. Van Pouderoyen, T. Eggert, K.E. Jaeger, B.W. Dijkstra, The crystal structure of *Bacillus subtili* lipase: a minimal α/β hydrolase fold enzyme1, J. Mol. Biol. 309 (2001) 215–226. https://doi.org/10.1006/jmbi.2001.4659.

[46] H.S. Yun, H.J. Park, J.C. Joo, Y.J. Yoo, Thermostabilization of *Bacillus subtilis* lipase A by minimizing the structural deformation caused by packing enhancement, J. Ind. Microbiol. Biotechnol. 40 (2013) 1223–1229. https://doi.org/10.1007/s10295-013-1330-2.

[47] T. Ozawa, Y. Hakamada, Y. Hatada, T. Kobayashi, T. Shirai, S. Ito, Thermostabilization

by replacement of specific residues with lysine in a *Bacillus* alkaline cellulase: building a structural model and implications of newly formed double intrahelical salt bridges, Protein Eng. Des. Sel. 14 (2001) 501–504. https://doi.org/10.1093/protein/14.7.501.

[48] I. Kufareva, R. Abagyan, Methods of protein structure comparison, in: A.J.W. Orry, R. Abagyan (Eds.), Homology Modeling, Springer, 857 (2011), pp. 231–257. https://doi.org/10.1007/978-1-61779-588-6_10.

[49] Y. Nakanishi, T. Saijo, Y. Wada, M. Maeshima, Mutagenic analysis of functional residues in putative substrate-binding site and acidic domains of vacuolar H^+-pyrophosphatase, J. Biol. Chem. 276 (2001) 7654–7660. https://doi.org/10.1074/jbc.M009743200.

[50] B. Folch, Y. Dehouck, M. Rooman, Thermo- and mesostabilizing protein interactions identified by temperature-dependent statistical potentials, Biophys. J. 98 (2010) 667–677. https://doi.org/10.1016/j.bpj.2009.10.050.

[51] K. Ohnishi, Y. Yoshida, J. Toita, J. Sekiguchi, Purification and characterization of a novel Lipolytic Enzyme from *Aspergillus oryzae*, J. Fermet. Bioeng. 78 (1994) 413–419. https://doi.org/10.1016/0922-338X(94)90039-6.

[52] A. Allali-Hassani, G.A. Wasney, I. Chau, B.S. Hong, G. Senisterra, P. Loppnau, Z. Shi, J. Moult, A.M. Edwards, C.H. Arrowsmith, H.W. Park, M. Schapira, M. Vedadi, A survey of proteins encoded by non-synonymous single nucleotide polymorphisms reveals a significant fraction with altered stability and activity, Biochem. J. 424 (2009) 15–26. https://doi.org/10.1042/BJ20090723.

[53] J.K. Song, J.S. Rhee, Simultaneous enhancement of thermostability and catalytic activity of phospholipase A1 by evolutionary molecular engineering, Appl. Environ. Microbiol. 66 (2000) 890–894. https://doi.org/10.1128/AEM.66.3.890-894.2000.

[54] T.Y. Kuo, C.C. Tsai, H.W. Fu, Enhanced mutant screening in one-step pcr-based multiple site-directed plasmid mutagenesis by introduction of silent restriction sites for structural and functional study of proteins, Biol. Proced. Online. 19 (2017) 12. https://doi.org/10.1186/s12575-017-0062-5.

[55] G. Abrusán, J.A. Marsh, Alpha Helices Are more robust to mutations than beta strands, PLOS Comput. Biol. 12 (2016) e1005242. https://doi.org/10.1371/journal.pcbi.1005242.

[56] A. Houde, A. Kademi, D. Leblanc, Lipases and their industrial applications: an overview, Appl. Biochem. Biotechnol. 118 (2004) 155–170. https://doi.org/10.1385/ABAB:118:1-3:155.

[57] D. Kundu, C. Hazra, A. Chatterjee, A. Chaudhari, S. Mishra, Extracellular biosynthesis of zinc oxide nanoparticles using *Rhodococcus pyridinivorans* NT2: Multifunctional textile finishing, biosafety evaluation and in vitro drug delivery in colon carcinoma, J. Photochem. Photobiol. B Biol. 140 (2014) 194–204. https://doi.org/10.1016/j.jphotobiol.2014.08.001.

[58] N. Rueda, J.C.S. dos Santos, C. Ortiz, R. Torres, O. Barbosa, R.C. Rodrigues, Á. Berenguer-Murcia, R. Fernandez-Lafuente, Chemical modification in the design of immobilized enzyme biocatalysts: Drawbacks and opportunities, Chem. Rec. 16 (2016) 1436–1455. https://doi.org/10.1002/tcr.201600007.

[59] M. Kashif, U. Hashim, M.E. Ali, S.M.U. Ali, M. Rusop, Z.H. Ibupoto, M. Willander, Effect of different seed solutions on the morphology and electrooptical properties of zno nanorods, J. Nanomater. 2012 (2012) 1–6. https://doi.org/10.1155/2012/452407.

[60] R.N. Moussawi, D. Patra, Nanoparticle self-assembled grain like curcumin conjugated ZnO: curcumin conjugation enhances removal of perylene, fluoranthene, and chrysene by

ZnO, Sci. Rep. 6 (2016) 24565. https://doi.org/10.1038/srep24565.

[61] H. Rodríguez-Tobías, G. Morales, A. Olivas, D. Grande, One-Pot Formation of ZnO- graft -Poly(D , L -Lactide) Hybrid Systems via Microwave-Assisted Polymerization of D , L -Lactide in the Presence of ZnO Nanoparticles, Macromol. Chem. Phys. 216 (2015) 1629–1637. https://doi.org/10.1002/macp.201500171.

[62] J.N. Hasnidawani, H.N. Azlina, H. Norita, N.N. Bonnia, S. Ratim, E.S. Ali, Synthesis of ZnO nanostructures using sol-gel method, Procedia Chem. 19 (2016) 211–216. https://doi.org/org/10.1016/j.proche.2016.03.095.

[63] T.R. Bastami, M.H. Entezari, Synthesis of manganese oxide nanocrystal by ultrasonic bath: effect of external magnetic field, Ultrason. Sonochem. 19 (2012) 830–840. https://doi.org/10.1016/j.ultsonch.2011.11.019.

[64] M.N. Zafar, Q. Dar, F. Nawaz, M.N. Zafar, M. Iqbal, M.F. Nazar, Effective adsorptive removal of azo dyes over spherical ZnO nanoparticles, J. Mater. Res. Technol. 8 (2019) 713–725. https://doi.org/10.1016/j.jmrt.2018.06.002.

[65] S. Cimitan, S. Albonetti, L. Forni, F. Peri, D. Lazzari, Solvothermal synthesis and properties control of doped ZnO nanoparticles, J. Colloid Interface Sci. 329 (2009) 73–80. https://doi.org/10.1016/j.jcis.2008.09.060.

[66] P. Jamdagni, P. Khatri, J.S. Rana, Green synthesis of zinc oxide nanoparticles using flower extract of Nyctanthes arbor-tristis and their antifungal activity, J. King Saud Univ. 30 (2018) 168–175. https://doi.org/10.1016/j.jksus.2016.10.002.

[67] S.A. Braham, F. Hussain, R. Morellon-Sterling, S. Kamal, J.F. Kornecki, O. Barbosa, D.E. Kati, R. Fernandez-Lafuente, Cooperativity of covalent attachment and ion exchange on alcalase immobilization using glutaraldehyde chemistry: Enzyme stabilization and

improved proteolytic activity, Biotechnol. Prog. 35 (2019) e2768. https://doi.org/10.1002/btpr.2768.

[68] F. Secundo, Conformational changes of enzymes upon immobilisation, Chem. Soc. Rev. 42 (2013) 6250–6261. https://doi.org/10.1039/C3CS35495D.

[69] S. Arana-Peña, C. Mendez-Sanchez, N.S. Rios, C. Ortiz, L.R.B. Gonçalves, R. Fernandez-Lafuente, New applications of glyoxyl-octyl agarose in lipases co-immobilization: Strategies to reuse the most stable lipase, Int. J. Biol. Macromol. 131 (2019) 989–997. https://doi.org/10.1016/j.ijbiomac.2019.03.163.

[70] E. Shah, P. Mahapatra, A. V. Bedekar, H.P. Soni, Immobilization of *Thermomyces lanuginosus* lipase on ZnO nanoparticles: mimicking the interfacial environment, RSC Adv. 5 (2015) 26291–26300. https://doi.org/10.1039/C5RA02249E.

[71] B.J. Jin, S. Im, S.Y. Lee, Violet and UV luminescence emitted from ZnO thin films grown on sapphire by pulsed laser deposition, Thin Solid Films. 366 (2000) 107–110. https://doi.org/10.1016/S0040-6090(00)00746-X.

[72] J. Shim, J.K. Kim, K.S. Lee, C.L. Lee, M. Ma, W.K. Choi, J.Y. Hwang, H.Y. Yang, B. Angadi, J.H. Park, K. Yu, D.I. Son, A facile chemical synthesis of ZnO@multilayer graphene nanoparticles with fast charge separation and enhanced performance for application in solar energy conversion, Nano Energy. 25 (2016) 9–17. https://doi.org/10.1016/j.nanoen.2016.04.031.

[73] A. Kumar, S. Arora, N. Mogha, S.S. Al-Deyab, Z.A. Ansari, S.G. Ansari, Glutathione coated Zinc oxide nanoparticles: a promising material for pesticide detection, Energy Environ. Focus. 2 (2013) 101–107. https://doi.org/10.1166/eef.2013.1034.

[74] E.H. Kisi, M.M. Elcombe, u parameters for the wurtzite structure of ZnS and ZnO using

powder neutron diffraction, Acta Crystallogr. Sect. C Cryst. Struct. Commun. 45 (1989) 1867–1870. https://doi.org/10.1107/S0108270189004269.

[75] Y. Chen, B. Xiao, J. Chang, Y. Fu, P. Lv, X. Wang, Synthesis of biodiesel from waste cooking oil using immobilized lipase in fixed bed reactor, Energy Convers. Manag. 50 (2009) 668–673. https://doi.org/10.1016/j.enconman.2008.10.011.

[76] R.C. Rodrigues, J.M. Bolivar, A. Palau-Ors, G. Volpato, M.A.Z. Ayub, R. Fernandez-Lafuente, J.M. Guisan, Positive effects of the multipoint covalent immobilization in the reactivation of partially inactivated derivatives of lipase from *Thermomyces lanuginosus*, Enzyme Microb. Technol. 44 (2009) 386–393. https://doi.org/10.1016/j.enzmictec.2009.02.009.

[77] S.Z. Mazlan, S.A. Hanifah, Effects of temperature and pH on immobilized laccase activity in conjugated methacrylate-acrylate microspheres, Int. J. Polym. Sci. 2017 (2017) 5657271. https://doi.org/10.1155/2017/5657271.

[78] N. Musa, W. Latip, R. Abd Rahman, A. Salleh, M. Mohamad Ali, Immobilization of an Antarctic Pseudomonas AMS8 lipase for low temperature ethyl hexanoate synthesis, Catalysts. 8 (2018) 234. https://doi.org/10.3390/catal8060234.

[79] M. Defaei, A. Taheri-Kafrani, M. Miroliaei, P. Yaghmaei, Improvement of stability and reusability of α-amylase immobilized on naringin functionalized magnetic nanoparticles: A robust nanobiocatalyst, Int. J. Biol. Macromol. 113 (2018) 354–360. https://doi.org/10.1016/j.ijbiomac.2018.02.147.

[80] K.V. Sajna, R.K. Sukumaran, H. Jayamurthy, K.K. Reddy, S. Kanjilal, R.B.N. Prasad, A. Pandey, Studies on biosurfactants from *Pseudozyma* sp. NII 08165 and their potential application as laundry detergent additives, Biochem. Eng. J. 78 (2013) 85–92.

https://doi.org/10.1016/j.bej.2012.12.014.

[81] S. Grbavčić, D. Bezbradica, L. Izrael-Živković, N. Avramović, N. Milosavić, I. Karadžić, Z. Knežević-Jugović, Production of lipase and protease from an indigenous *Pseudomonas aeruginosa* strain and their evaluation as detergent additives: Compatibility study with detergent ingredients and washing performance, Bioresour. Technol. 102 (2011) 11226–11233. https://doi.org/10.1016/j.biortech.2011.09.076.

[82] I.B.B. Romdhane, A. Fendri, Y. Gargouri, A. Gargouri, H. Belghith, A novel thermoactive and alkaline lipase from *Talaromyces thermophilus* fungus for use in laundry detergents, Biochem. Eng. J. 53 (2010) 112–120. https://doi.org/10.1016/j.bej.2010.10.002.

Figure Captions

Fig. 1. Scheme of ZnO nanoparticle synthesis, coating and lipase immobilization.

Fig. 2. (A) Graphical representation of relative abundance analysis of amino acids contributing to protein thermostability and mesostability. Blue color bars are the amino acids contributing positively for protein thermostability whereas, green blue color bars are the amino acids contributing negatively for protein thermostability and *vice versa* for protein mesostability. (B) Ranking of amino acids according to their relative priority vectors calculated through generated reciprocal pairwise comparison matrix.

Fig. 3. Validation of mutant lipases through various *in silico* approaches. (A) Structural representation of selected mutational hotspots in *Bacillus subtilis* lipase. (B) Analysis of rank difference based on selected significant amino acids in mutant lipases (bsl_the1, bsl_the2 and bsl_the3) with respect to wild-type lipase (bsl_wt) using AHP model. Mutation can increase or decrease the content of these amino acids. Green highlighted amino acids showed increased

contents whereas, orange highlighted amino acids showed decreased contents after attaining mutations and equal weighted amino acids are remained uncolored. (C) Validation of chosen mutations using various mutation prediction servers. (D) Analyzing superimposition of mutant lipases with respect to wild-type lipase to calculate the RMSD values. (E) *p*-NPO (C8) docking with lipase variants and enumeration of docking parameters. (F) Structure validation of wild-type and mutant lipases through Ramachandran plot analysis to identify the residue percentage in the most favored region. (G) Analysis of unique contact formed in mutant lipases through generation of 2D contact maps. In contact maps, pink dots represents unique bonds in wild-type lipase whereas, green dots represents unique bonds in mutant lipase and black dots are for common bonds. The number of unique contacts in wild-type and mutant lipases has been represented graphically in the figure.

Fig. 4. Relative activity of lipase variants for identifying the (A) optimum temperature, (B) temperature stability (at 50 °C), (C) optimum pH, (D) pH stability (at pH ; (E) thermograph of wild-type and mutant lipases.

Fig. 5. Effect of various (A) surfactants, (B) oxidizing agents and (C) commercial detergents on lipases. All experiments were conducted in triplicate and represented as mean ± SD (error bars); *p*-value < 0.05.

Fig. 6. (A-C) FESEM, (D-F) TEM, and (G-I) DLS analysis of as-synthesized ZnO, ZnO-bsl_wt and ZnO-bsl_the3.

Fig. 7. (A) UV-Vis, (B) FT-IR, (C) XRD and (D) DSC-TGA analysis of wild-type and mutant lipases.

Fig. 8. Comparative analysis of (A) reusability and (B) storage stability of immobilized wild-type lipases. All experiments were conducted in triplicate and the data have been represented as mean ± SD (error bars).

Fig. 9. (A) Effect of various surfactant, detergents and oxidizing agents on lipase after immobilization. Optimization of oil removal for (B-C) lipase concentrations, (D-E) detergent concentrations, (F-G) washing temperature and (H-I) washing time by wild-type and thermostable lipase mutant. All experiments were conducted in triplicate and the data have been represented as mean ± SD (error bars); p-value < 0.05.

Fig. 10. Photographs and FESEM micrographs of (A) oil and (B) grease stained and destained fabric.

Table 1

Validation of ranking models by blind test analysis.

Blind test set	**No. of proteins**	**Mean Rank**	**Rank Difference**	**Accuracy (%)**
1st	100 Thermophilic proteins	0.540	0.09	96.0
	100 Mesophilic proteins	0.450		
2nd	100 Mesophilic proteins	0.4998	0.0002	-
	100 Mesophilic proteins	0.5000		

Table 2

Enzyme kinetic parameters of the wild-type and mutant lipases.

Lipases	**Enzyme concentration (mg mL^{-1})**	**Specific activity (U mg^{-1})**	**Enzyme activity (U mL^{-1})**	**K_m (μM)**	**Turnover number, k_{cat} (sec^{-1})**	**Catalytic efficiency, k_{cat}/K_m (μM^{-1} sec^{-1})**
bsl_wt	0.01	1583	15.83	94	511	5.43
bsl_the1	0.01	1725	17.25	98	557	5.68
bsl_the2	0.01	1891	18.91	106	610	5.76
bsl_the3	0.01	2396	23.96	115	773	6.72

Table 3

Percentage composition of secondary structures in wild-type and mutant lipases.

Lipases	α-helices	β-sheets	Turns	Random coils
bsl_wt (database)	46.93	21.79	19.55	11.73
bsl_wt	46.87	21.56	18.47	13.09
bsl_the1	53.56	23.86	20.19	2.37
bsl_the2	56.43	27.05	15.91	0.58
bsl_the3	55.99	27.30	13.11	3.58

Table 4

Kinetics and physicochemical parameters of immobilized lipases.

Parameters	ZnO-bsl_wt	ZnO-bsl_the3
Lipase used for immobilization, E_0(mg mL^{-1})	10.0	10.0
Lipase in filtrate after immobilization, E_1(mg mL^{-1})	1.75	1.15
Immobilization efficiency (%)	82.5	88.5
Activity of immobilized lipase, Y_1 (U mL^{-1})	113.9	190.4
Activity of free lipase, Y_0 (U mL^{-1})	158.3	239.6
Immobilization yield (%)	71.9	79.5
Optimum temperature (°C)	40.0	60.0
Optimum pH	8.5	10.0

Highlights

- Analysis of differentiating amino acids from thermophilic and mesophilic proteins.
- Prioritizing amino acid attributes for attaining thermostabilizing mutations.
- Mesophilic *Bacillus subtilis* lipase chosen to enhance thermostability.
- Covalent immobilization of lipases on functionalized ZnO nanoparticles.
- Immobilized engineered lipases applied in detergent formulation.

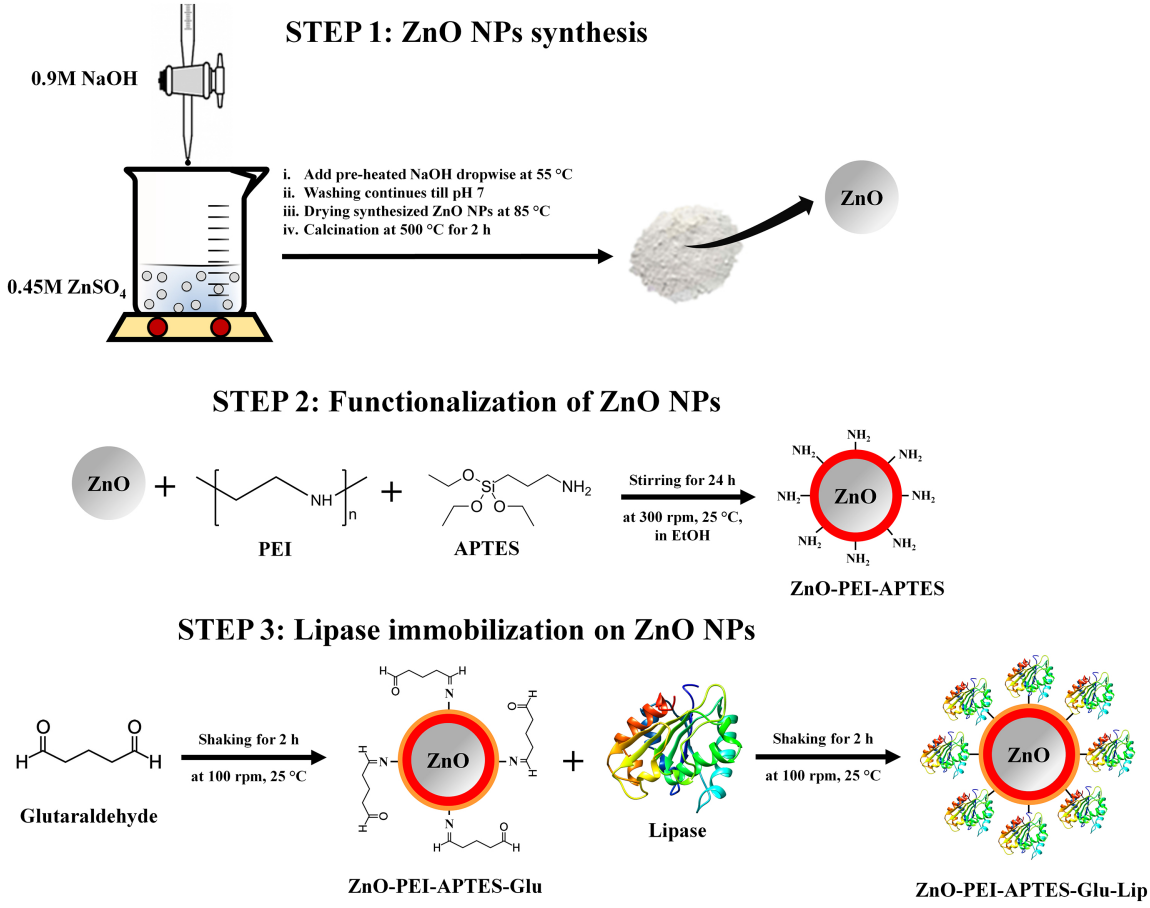
STEP 1: ZnO NPs synthesis
0.9M NaOH
0.45M ZnSO4
i. Add pre-heated NaOH dropwise at 55 °C
ii. Washing continues till pH 7
iii. Drying synthesized ZnO NPs at 85 °C
iv. Calcination at 500 °C for 2 h
ZnO
STEP 2: Functionalization of ZnO NPs
ZnO
PEI
APTES
Stirring for 24 h
at 300 rpm, 25 °C,
in EtOH
ZnO-PEI-APTES
STEP 3: Lipase immobilization on ZnO NPs
ZnO-PEI-APTES
Glutaraldehyde
Shaking for 2 h
at 100 rpm, 25 °C
ZnO-PEI-APTES-Glu
Lipase
Shaking for 2 h
at 100 rpm, 25 °C
ZnO-PEI-APTES-Glu-Lip

Figure 1

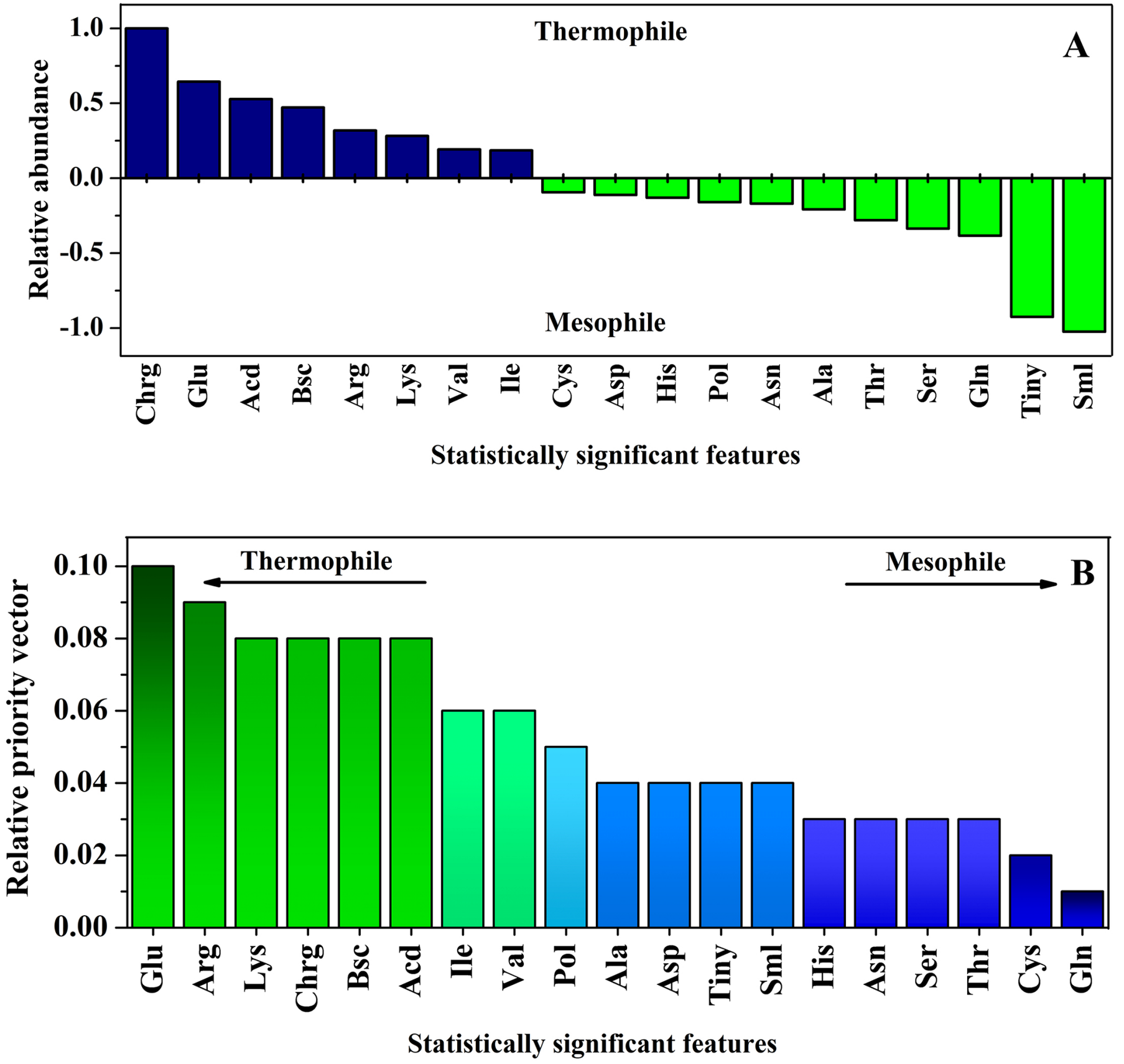
A
Thermophile
Mesophile
Relative abundance
1.0
0.5
0.0
-0.5
-1.0
Chrg
Glu
Acd
Bsc
Arg
Lys
Val
Ile
Cys
Asp
His
Pol
Asn
Ala
Thr
Ser
Gln
Tiny
Sml
Statistically significant features
B
Thermophile
Mesophile
Relative priority vector
0.10
0.08
0.06
0.04
0.02
0.00
Glu
Arg
Lys
Chrg
Bsc
Acd
Ile
Val
Pol
Ala
Asp
Tiny
Sml
His
Asn
Ser
Thr
Cys
Gln
Statistically significant features

Figure 2

A. Mutational hotspots in *Bacillus subtilis* lipase

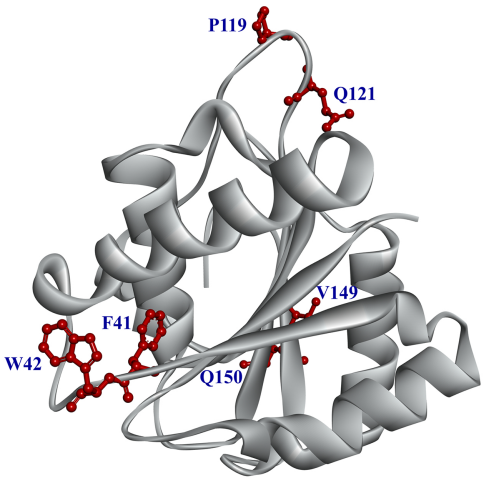

B. Prediction and validation of mutations using AHP generated model

Lipase	Point mutations	Change in content (%) of attributes in lipase after mutations																		Rank difference ($R_{mut} - R_{wt}$)
		Ala	Cys	Asp	Glu	His	Ile	Lys	Asn	Gln	Arg	Ser	Thr	Val	Tiny	Sml	Pol	Chrg	Bsc	Acd	
bsl_wt	-	6.63	0	4.97	1.66	2.76	5.52	6.08	9.39	3.31	2.76	7.18	5.52	9.39	32.60	58.56	43.65	18.23	11.60	6.63	-
bsl_the1	V149K, Q150E	6.63	0	4.97	2.21	2.76	5.52	6.63	9.39	2.95	2.76	7.18	5.52	8.84	32.60	58.56	44.39	19.33	12.15	7.19	0.510 – 0.489 = **0.021**
bsl_the2	F41K, W42E, V149K, Q150E	6.63	0	4.97	2.76	2.76	5.52	7.18	9.39	2.95	2.76	7.18	5.52	8.84	32.60	58.56	45.11	20.44	12.70	7.73	0.522 – 0.479 = **0.043**
bsl_the3	F41K, W42E, P119E, Q121K, V149K, Q150E	6.63	0	4.97	3.31	2.76	5.52	7.73	9.39	2.21	2.76	7.18	5.52	8.84	32.60	57.46	45.86	21.55	13.26	8.29	0.531 – 0.469 = **0.062**

Increasing attributes *w.r.t.* bsl_wt Decreasing attributes *w.r.t.* bsl_wt

C. Cross validation of predicted mutations using online tools

Point mutations	HOTSPOT	SCIDE	CUPSAT	I-MUTANT	I-PTREE STAB	ERIS	WET STAB
F41K	S	S	S	D	S	S	S
W42E	S	S	S	D	S	D	S
P119E	S	S	S	S	S	S	S
Q121K	S	S	S	S	S	S	S
V149K	S	S	S	S	S	S	S
Q150E	S	S	S	D	S	S	S

S = Stabilizing mutation; D = Destabilizing mutation

D. Superimposition analysis

Mutant	Superimposition (RMSD)
bsl_the1	0.225
bsl_the2	0.234
bsl_the3	0.242

E. Docking analysis using *p*-nitrophenyl octanoate (C8)

Lipase	Binding Energy (kcal/mol)	Inhibition Constant (μM)	Unbound Extended Energy (kcal/mol)
bsl_wt	-5.99	30.71	-0.49
bsl_the1	-6.11	26.53	-0.18
bsl_the2	-6.36	21.69	-0.28
bsl_the3	-7.61	20.52	-0.87

F. Ramachandran Plot analysis

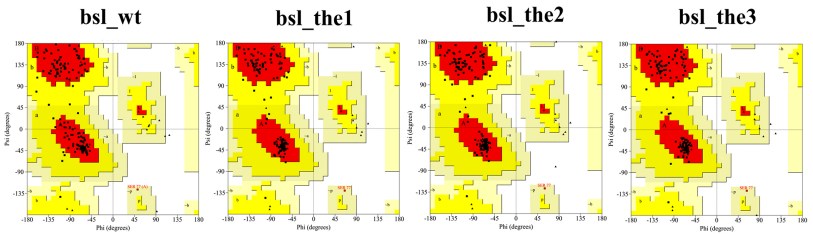

Lipase	bsl_wt	bsl_the1	bsl_the2	bsl_the3
Total residue (except Gly and Pro)	153	153	153	153
Residues in favoured region	135	140	142	143
% residues favoured region	88.2	91.5	92.8	93.5

G. Contact map analysis

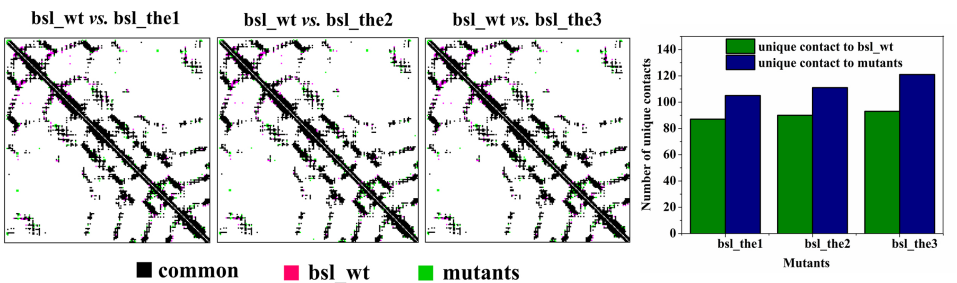

Figure 3

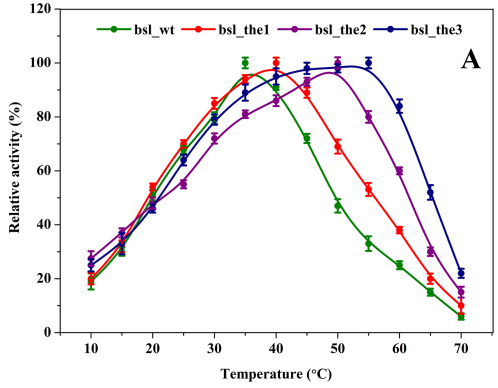
bsl_wt
bsl_the1
bsl_the2
bsl_the3
A
Relative activity (%)
Temperature (°C)

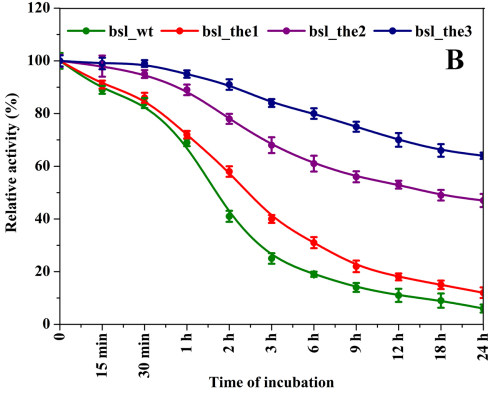
bsl_wt
bsl_the1
bsl_the2
bsl_the3
B
Relative activity (%)
0
15 min
30 min
1 h
2 h
3 h
6 h
9 h
12 h
18 h
24 h
Time of incubation

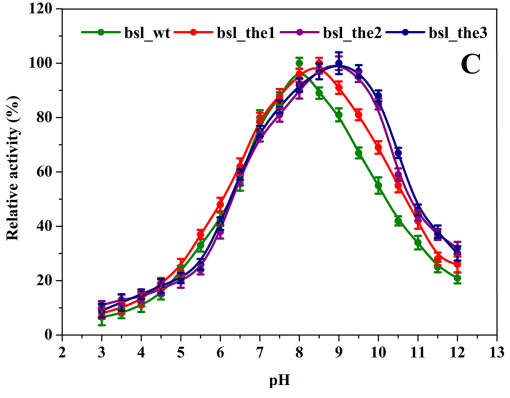
bsl_wt
bsl_the1
bsl_the2
bsl_the3
C
Relative activity (%)
pH

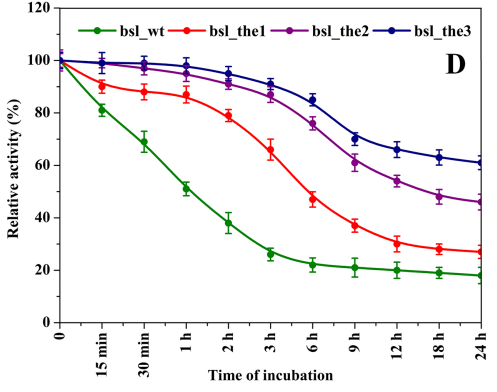
bsl_wt
bsl_the1
bsl_the2
bsl_the3
D
Relative activity (%)
0
15 min
30 min
1 h
2 h
3 h
6 h
9 h
12 h
18 h
24 h
Time of incubation

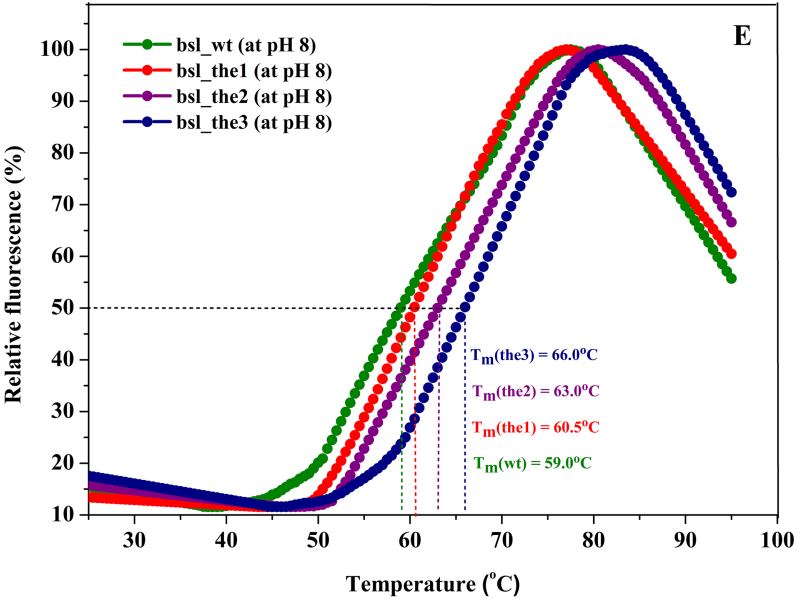
bsl_wt (at pH 8)
bsl_the1 (at pH 8)
bsl_the2 (at pH 8)
bsl_the3 (at pH 8)
E
Relative fluorescence (%)
Tm(the3) = 66.0°C
Tm(the2) = 63.0°C
Tm(the1) = 60.5°C
Tm(wt) = 59.0°C
Temperature (°C)

Figure 4

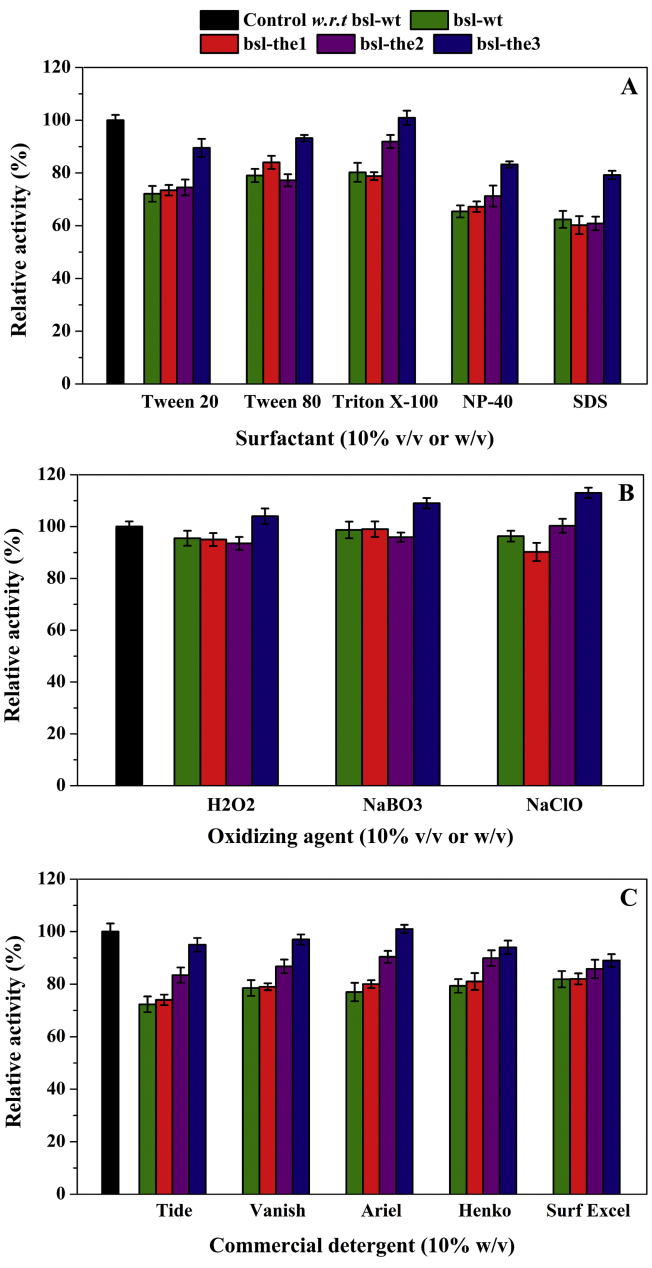
Control w.r.t bsl-wt
bsl-wt
bsl-the1
bsl-the2
bsl-the3
A
Relative activity (%)
120
100
80
60
40
20
0
Tween 20
Tween 80
Triton X-100
NP-40
SDS
Surfactant (10% v/v or w/v)
B
Relative activity (%)
H2O2
NaBO3
NaClO
Oxidizing agent (10% v/v or w/v)
C
Relative activity (%)
Tide
Vanish
Ariel
Henko
Surf Excel
Commercial detergent (10% w/v)

Figure 5

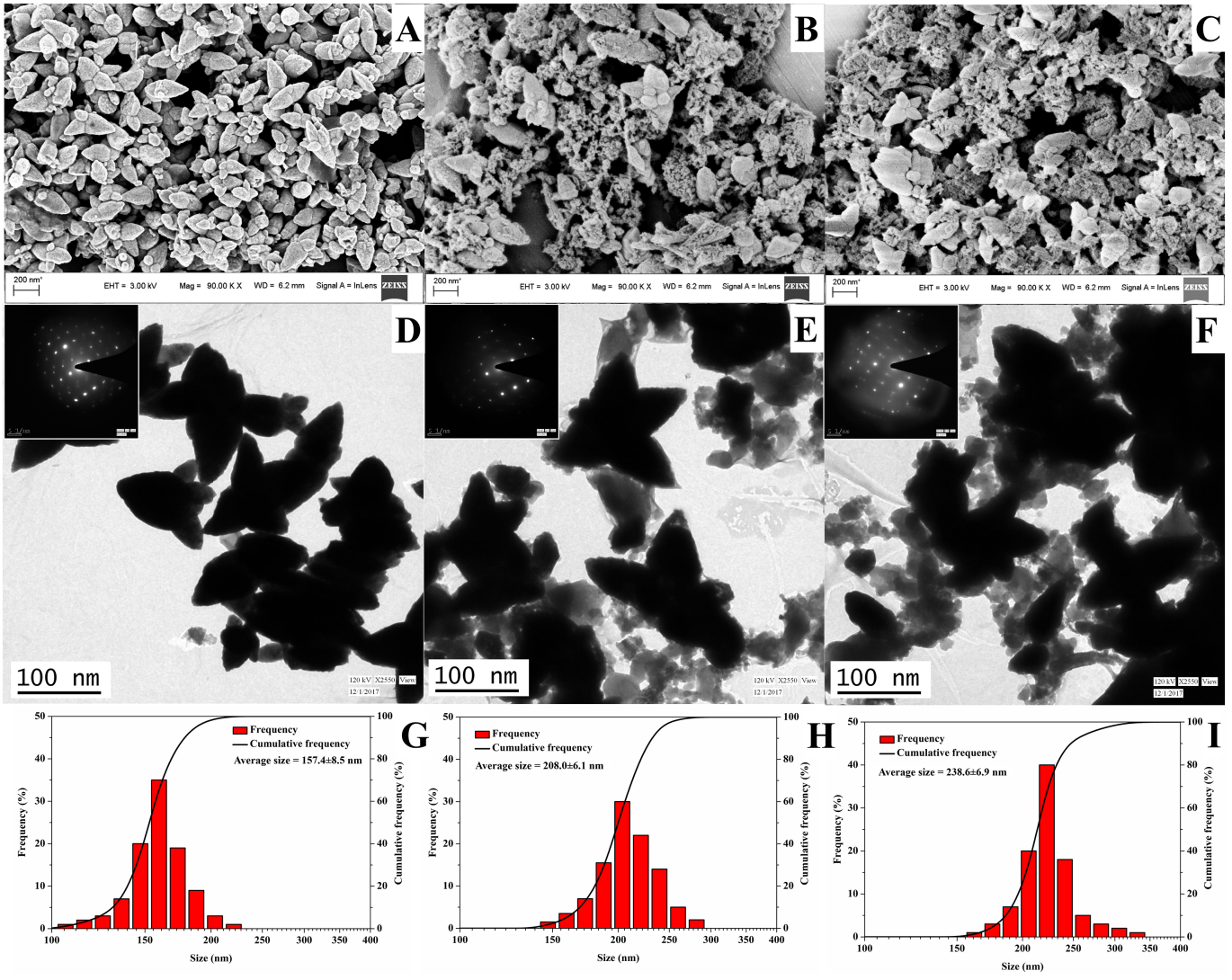
A
B
C
200 nm*
EHT = 3.00 kV
Mag = 90.00 K X
WD = 6.2 mm
Signal A = InLens
ZEISS
D
E
F
100 nm
120 kV X2550 View
12/1/2017
G
H
I
Frequency
Cumulative frequency
Average size = 157.4±8.5 nm
Average size = 208.0±6.1 nm
Average size = 238.6±6.9 nm
Frequency (%)
Cumulative frequency (%)
Size (nm)

Figure 6

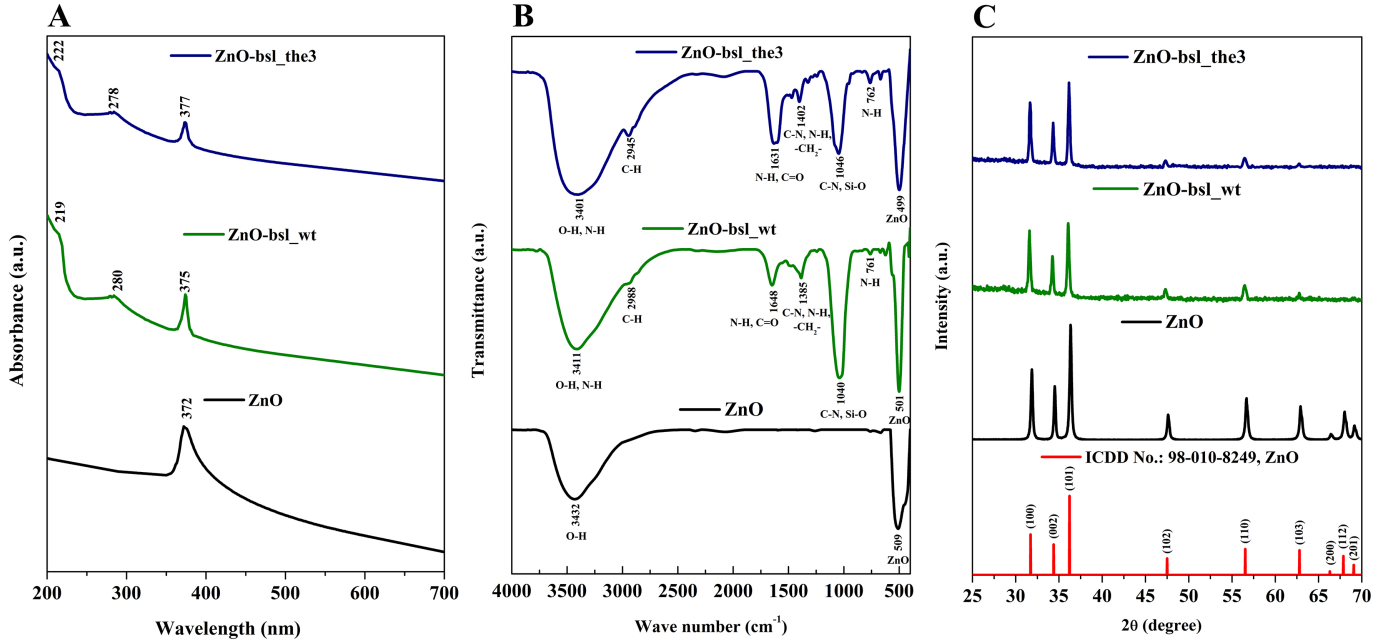
A
ZnO-bsl_the3
222
278
377
ZnO-bsl_wt
219
280
375
ZnO
372
Absorbance (a.u.)
200
300
400
500
600
700
Wavelength (nm)
B
ZnO-bsl_the3
3401
O-H, N-H
2945
C-H
1631
N-H, C=O
1402
C-N, N-H2
-CH2-
1046
C-N, Si-O
762
N-H
499
ZnO
ZnO-bsl_wt
3411
O-H, N-H
2988
C-H
1648
N-H, C=O
1385
C-N, N-H2
-CH2-
1040
C-N, Si-O
761
N-H
501
ZnO
ZnO
3432
O-H
509
ZnO
Transmittance (a.u.)
4000
3500
3000
2500
2000
1500
1000
500
Wave number (cm-1)
C
ZnO-bsl_the3
ZnO-bsl_wt
ZnO
ICDD No.: 98-010-8249, ZnO
(100)
(002)
(101)
(102)
(110)
(103)
(200)
(112)
(201)
Intensity (a.u.)
25
30
35
40
45
50
55
60
65
70
2θ (degree)

Figure 7

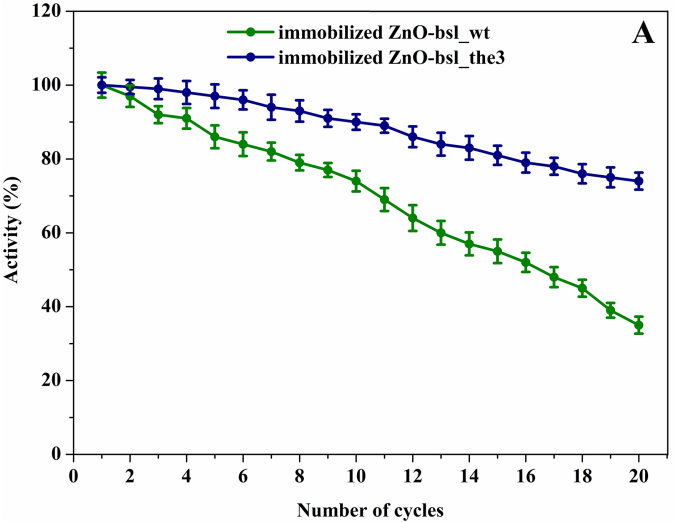
A
immobilized ZnO-bsl_wt
immobilized ZnO-bsl_the3
Activity (%)
Number of cycles
0
20
40
60
80
100
120
0
2
4
6
8
10
12
14
16
18
20

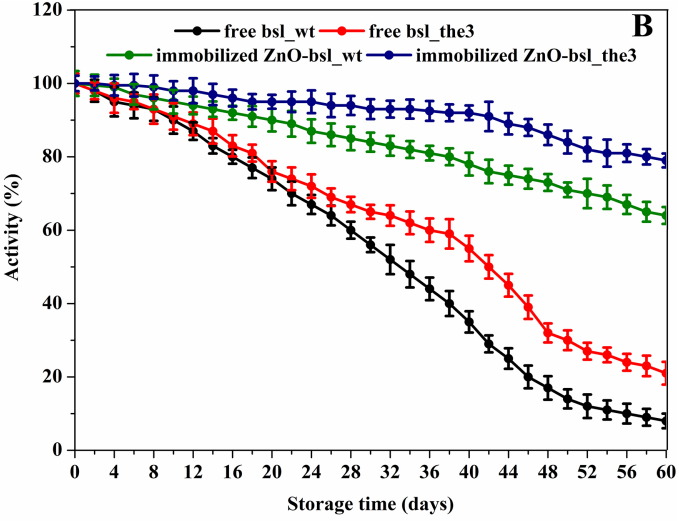
B
free bsl_wt
free bsl_the3
immobilized ZnO-bsl_wt
immobilized ZnO-bsl_the3
Activity (%)
Storage time (days)
0
20
40
60
80
100
120
0
4
8
12
16
20
24
28
32
36
40
44
48
52
56
60

Figure 8

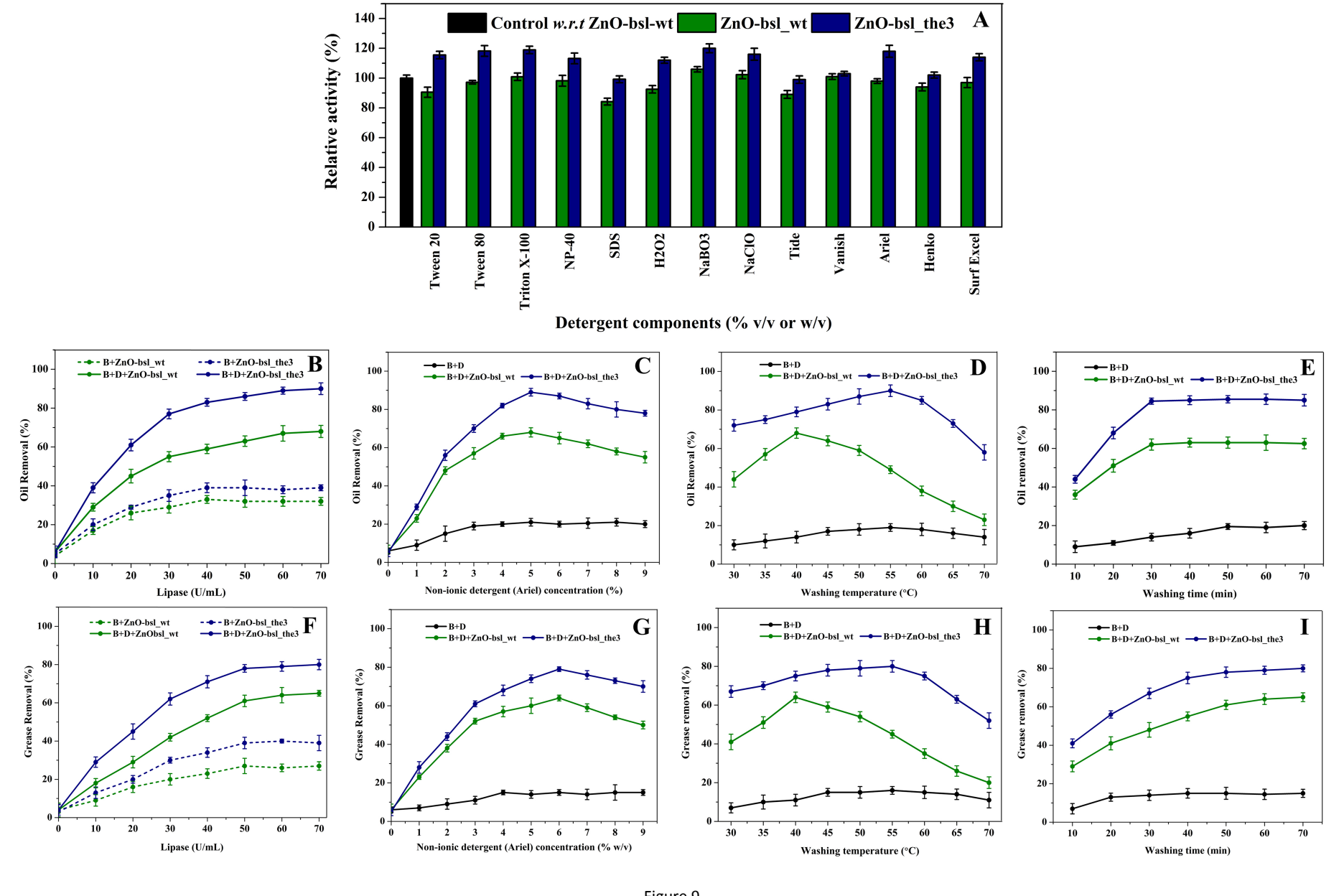
A
Control w.r.t ZnO-bsl-wt
ZnO-bsl_wt
ZnO-bsl_the3
Relative activity (%)
Tween 20
Tween 80
Triton X-100
NP-40
SDS
H2O2
NaBO3
NaClO
Tide
Vanish
Ariel
Henko
Surf Excel
Detergent components (% v/v or w/v)
B
B+ZnO-bsl_wt
B+ZnO-bsl_the3
B+D+ZnO-bsl_wt
B+D+ZnO-bsl_the3
Oil Removal (%)
Lipase (U/mL)
C
B+D
Non-ionic detergent (Ariel) concentration (%)
D
Washing temperature (°C)
E
Oil removal (%)
Washing time (min)
F
B+D+ZnOBsl_wt
Grease Removal (%)
G
Non-ionic detergent (Ariel) concentration (% w/v)
H
Grease removal (%)
I

Figure 9

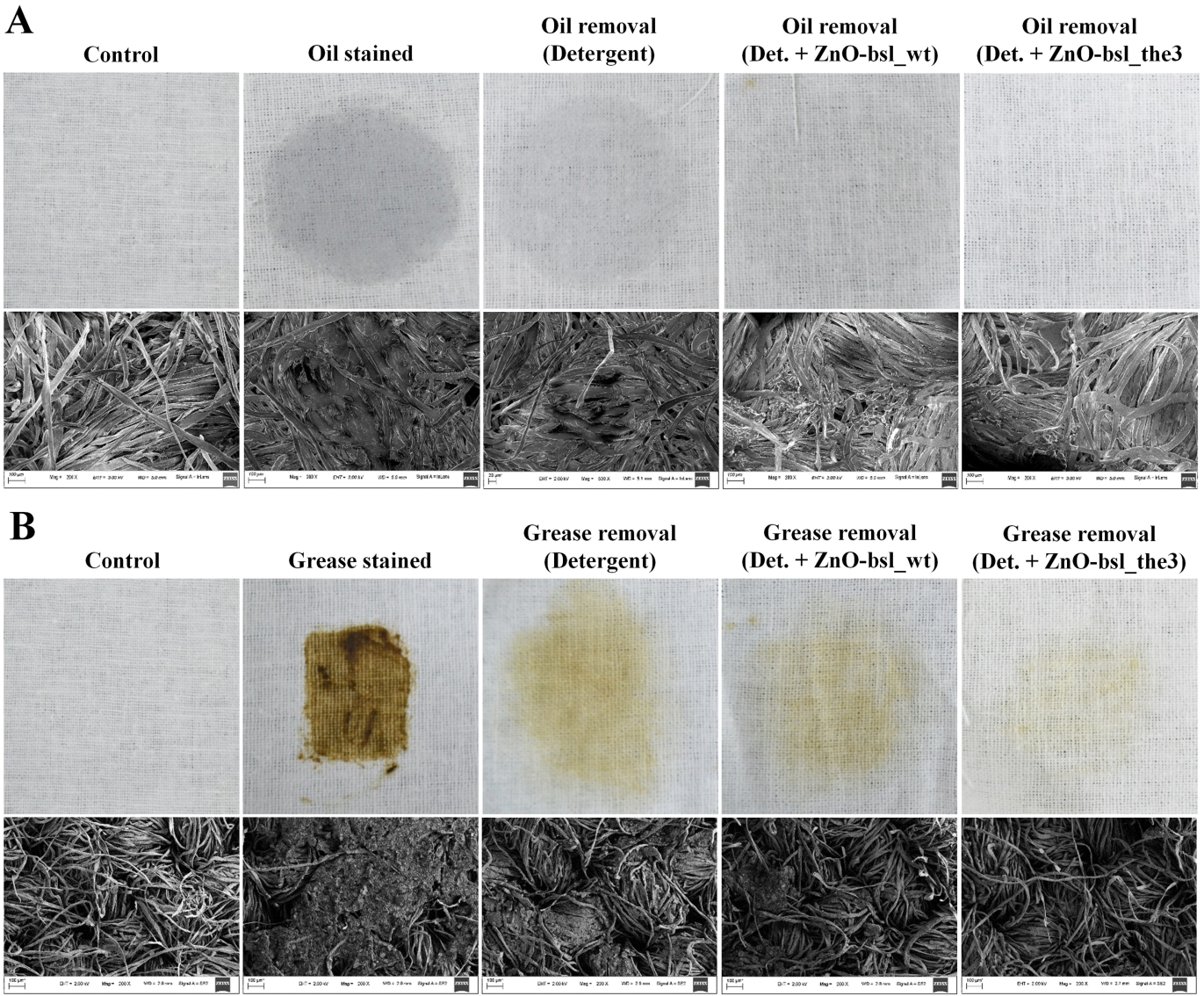
A
Control
Oil stained
Oil removal (Detergent)
Oil removal (Det. + ZnO-bsl_wt)
Oil removal (Det. + ZnO-bsl_the3
B
Control
Grease stained
Grease removal (Detergent)
Grease removal (Det. + ZnO-bsl_wt)
Grease removal (Det. + ZnO-bsl_the3)

Figure 10